
PERGAMON

Journal of the Mechanics and Physics of Solids
50 (2002) 1231–1268

JOURNAL OF THE
MECHANICS AND
PHYSICS OF SOLIDS

www.elsevier.com/locate/jmps

Subsonic and intersonic mode II crack propagation with a rate-dependent cohesive zone

O. Samudrala[a], Y. Huang[b], A.J. Rosakis[a,*]

[a] *Graduate Aeronautical Laboratories, California Institute of Technology, Mail Stop 105-50, Pasadena, CA 91125, USA*

[b] *Department of Mechanical and Industrial Engineering, University of Illinois at Urbana-Champaign, Urbana, IL 61801, USA*

Received 9 February 2001; accepted 16 October 2001

Abstract

A recent experimental study has demonstrated the attainability of intersonic shear crack growth along weak planes in otherwise homogeneous, isotropic, linear elastic solids subjected to remote loading conditions (Rosakis et al., Science 284 (5418) (1999) 1337). The relevant experimental observations are summarized briefly here and the conditions governing the attainment of intersonic crack speeds are examined. Motivated by experimental observations, subsonic and intersonic mode II crack propagation with a rate-dependent cohesive zone is subsequently analyzed. A cohesive law is assumed, wherein the cohesive shear traction is either a constant or varies linearly with the local sliding rate. Complete decohesion is assumed to occur when the crack tip sliding displacement reaches a material-specific critical value. Closed form expressions are obtained for the near-tip fields. With a cohesive zone of finite size, it is found that the dynamic energy release rate is finite through out the intersonic regime. Crack tip stability issues are addressed and favorable speed regimes are identified. The influence of shear strength of the crack plane and of a rate parameter on crack propagation behavior is also investigated. The isochromatic fringe patterns predicted by the analytical solution are compared with the experimental observations of Rosakis et al. (1999) and comments are made on the validity of the proposed model.

Keywords: A. Dynamic fracture; Crack propagation; Intersonic speeds; B. Rate-dependent cohesive law; C. Analytic functions

* Corresponding author. Tel.: +1-626-395-4523; fax: +1-626-449-6359.
E-mail addresses: rosakis@aero.caltech.edu, rosakis@atlantis.caltech.edu (A.J. Rosakis).

0022-5096/02/$ - see front matter
PII: S0022-5096(01)00129-6

1. Introduction

For remotely loaded mode I cracks in homogeneous, isotropic, linear elastic solids, the theoretical upper limit on the propagation speed v is the Rayleigh wave speed (c_R) of the material (Freund, 1990; Broberg, 1999a). The energy flux into the crack tip region vanishes at c_R and at higher speeds no analytical solution can be found with positive energy flux into the tip (Broberg, 1989). Indeed, positive energy flux is required because crack growth involves material separation, which is an energy-consuming process, and hence a necessary condition for propagation of a crack is that energy be supplied from the outer stress field to the crack tip region.

However, experimental observations in the laboratory typically show mode I crack speeds that are less than 60% of c_R (Fineberg and Marder, 1999). At about 30–40% of c_R, the micro-branching instability sets in, whereby the crack follows a wavy path producing increasingly rough fracture surfaces and repeatedly attempts to branch (Ramulu and Kobayashi, 1985; Ravichandar and Knauss, 1984a; Gao, 1993). Eventually, successful branching into multiple cracks occurs at speeds much below c_R, thus making the theoretical limit inaccessible. Also the height of the process region (for e.g., zone of micro-cracking) increases substantially at high fracture speeds, indicating a strong increase in the fracture energy required to sustain propagation at these speeds (Ravichandar and Knauss, 1984b; Johnson, 1992). Knauss and his coworkers have shown that if the height of the process region can be restrained to a thin layer along the crack path, thus suppressing branching, then crack speeds can approach the theoretical limiting speed, c_R (Lee and Knauss, 1989; Washabaugh and Knauss, 1994). They observed mode I cracks along a weak plane between two identical brittle solids, asymptotically approaching the theoretical limit c_R, as the cohesive strength of the plane was reduced. The only scenario in which a mode I crack can attain intersonic or supersonic speeds is when loading is applied directly at the crack tip. Winkler et al. (1970), Curran et al. (1970) reported supersonic crack growth along weak crystallographic planes of potassium chloride, where the crack tip was loaded by laser-induced expanding plasma. The crack speeds observed coincided with the measured plasma expansion speeds, implying that the situation was similar to a crack being driven by a supersonic wedge.

For remotely loaded mode II cracks (prescribed to propagate in their own plane), crack speeds below c_R (subRayleigh) as well as those in the intersonic regime (speeds between the shear wave speed, c_s and the longitudinal wave speed, c_l) are permissible from energetic considerations similar to the mode I case. The crack speed regime between c_R and c_s is forbidden. As a result, such cracks may either be purely sub-Rayleigh or purely intersonic, but may not transition between the two regimes with a continuous variation of crack speed. Hence the upper limit on the propagation speed (according to the classical interpretation based on a linear elastic constitutive description) for a remotely loaded mode II crack is c_l (Broberg, 1996).

Propagating mode II cracks are usually not observed (experimentally) in homogeneous isotropic solids. A crack subjected to mode II or mixed mode loading, curves or kinks and propagates in a direction that maintains locally pure mode I conditions at the tip (Cotterell and Rice, 1980; Nematnasser and Horii, 1982; Hutchinson and

Suo, 1992). Mode II crack growth in homogeneous isotropic solids can occur, if high compressive ambient stresses are acting on the body, preventing crack opening (Melin, 1986; Broberg, 1987). Directional stability of mode II cracks may also be sustained, if they propagate along a weak layer. A prime example of dynamically growing mode II cracks are earthquake fault ruptures which occur in the presence of high ambient compressive and shear pre-stresses and most often also propagate along pre-existing weak fault planes in the earth's crust. Ruptures on shallow crustal faults are estimated to run at average speeds close to c_s of crustal rocks, although evidence has accumulated over the years, of intersonic rupture speeds at least over a portion of the faulting (Archuleta, 1984; Spudich and Cranswick, 1984; Olsen et al., 1997; Hernandez et al., 1999; Ellsworth and Celebi, 1999; Bouchon et al., 2000, 2001). Rosakis et al. (1999, 2000), provided the first unambiguous evidence of intersonic mode II cracks in the laboratory. A single edge-notch oriented along a weak joint between two identical plates of Homalite-100, a brittle polyester resin, was subjected to dynamic shear loading by a projectile fired from a gas gun. A shear crack initiating from the notch was observed to propagate at intersonic speeds and radiate shear Mach waves.

Most of the early analytical and numerical work on dynamic shear crack propagation has appeared in the seismological literature. In probably the first study on intersonic shear cracks, Burridge (1973) analyzed the problem of a mode II crack growing self-similarly from zero initial length along an interface between two identical half-spaces held together by Coulomb frictional contact and subjected to pre-imposed uniform normal and shear stresses. The crack front was defined to be the loci of points where the shear stress drops abruptly from the limiting static friction value to the dynamic friction value. He found that for subsonic crack speeds, a positive peak in shear stress propagating along with the shear wave front, appears ahead of the crack tip. This peak in shear stress is observed to increase in magnitude as the crack speed increases and he postulated that it might lead to a secondary slip zone in front of the main crack tip provided the limiting static friction is small. He argued that a shear crack on such an interface will propagate at c_R and if the limiting static friction is small, it would propagate at c_l. He also noted that the crack tip stress singularity for intersonic mode II cracks is less than $\frac{1}{2}$ and that it is a function of crack speed. Andrews (1976) analyzed numerically, the problem of transient symmetric expansion of a mode II crack propagating along a prescribed path with a slip weakening cohesive zone (Ida, 1972; Palmer and Rice, 1973), under the action of a uniform remote shear stress. Corroborating Burridge's prediction, he found that the expanding shear crack rapidly accelerates to speeds close to c_R, and if the limiting static friction is not high enough, it initiates a secondary slip zone in front of it, which coalesces with the main crack and the combination was found to propagate at speeds around $1.5c_s$. His observation describes one possible mechanism for a subsonic shear crack to cross the forbidden speed regime between c_R and c_s. He pointed out that for intersonic cracks, where the crack tip stress singularity is less than $\frac{1}{2}$, a non-zero fracture energy is supported only for the case where the stress drop is not abrupt, i.e., the crack tip region must have a finite extent. Das and Aki (1977) analyzed transient mode II crack expansion in an infinite, isotropic, homogeneous, elastic solid under uniform remote shear stress using a boundary integral method. The crack tip was modeled as a structureless point and

dynamic friction was assumed to act on the crack faces. Using a critical stress criterion, they confirmed the numerical results of Andrews (1976).

Freund (1979) obtained the asymptotic stress and particle velocity fields around a steady state, intersonic mode II crack, constrained to propagate along a straight line path. Since mode II cracks usually do not propagate along straight line paths, this restriction models the existence of a line of lower toughness in an otherwise homogeneous solid, a situation that may make mode II crack growth physically possible. He showed that the stress field predicts two Mach waves radiating from the crack tip. Stresses are singular not only at the crack tip, but all along the Mach fronts, with the same order of singularity as that at the tip. In addition, across the Mach front, the normal stress perpendicular to the front is continuous, where as the shear stress suffers an infinite jump. Hence these fronts are shear Mach waves. He also commented upon the curious speed of $\sqrt{2}c_s$, at which an intersonic crack behaves "subsonic-like" and the two trailing Mach waves disappear. He investigated the problem of transient symmetric expansion of a mode II crack under remote shear stress which was studied numerically by Andrews (1976) and Das and Aki (1977). Using a critical stress criterion, he concluded that the terminal speed for a subRayleigh mode II crack is c_R, and that an intersonic mode II crack would begin to grow at a speed greater than $\sqrt{2}c_s$ and would quickly accelerate to c_l. Burridge et al. (1979) investigated the stability of a steady-state mode II semi-infinite crack with a slip-weakening cohesive zone driven by a point load acting on the crack faces a finite distance from the tip. They solved the governing integral equation numerically and concluded that, for a dynamic mode II crack, the crack speed regimes $v < c_R$ and $c_s < v < \sqrt{2}c_s$ are inherently unstable, the speed regime $\sqrt{2}c_s < v < c_l$ is stable and that the speed regime $c_R < v < c_s$ is forbidden.

Rice (1980), Das (1985) and Dmowska and Rice (1986) summarized the literature on dynamic shear crack propagation and its application to modeling the earthquake source process. Georgiadis (1986) investigated the nature of stress singularity for a steady-state mode II intersonic crack and confirmed Freund's result. Broberg (1989) gave an elegant summary of the admissible crack speed regimes for mode I, mode II and mode III cracks (all propagating along a pre-determined straight line path), based on the requirement of a positive energy flux to the crack tip region. Broberg (1994, 1995) also solved analytically the problem of a self-similar intersonic mode II crack expanding symmetrically from zero initial length under the action of a remote uniform shear stress. He showed that the dynamic energy release rate depends on the extent of the process region as $(d/a)^{(1-2q)}$, where d is the extent of the process region, a is the crack length and q is the speed-dependent crack tip stress singularity. Except for $v=\sqrt{2}c_s$, where $q=\frac{1}{2}$, a vanishing process region predicts a vanishing energy flux into the tip. He assumed a Barenblatt-type process region near the crack tip and computed the energy flux into the intersonic crack tip region. For the chosen process region type, he showed that the requirement of constant fracture energy (critical dynamic energy release rate), independent of crack speed, would accelerate an intersonic crack all the way up to c_l. He also solved the problem of an accelerating semi-infinite intersonic mode II crack (Broberg, 1999b). Johnson (1990) showed that steady-state unidirectional mode II crack growth is possible in earthquake events, provided, one of the leading

edges associated with an initially extending rupture front, encounters a barrier (region of high shear strength). In his finite element simulations, he observed terminal speeds close to c_l.

Some of the recent analytical and numerical work on dynamic shear cracks was motivated by the experiments of Rosakis and his coworkers on intersonic crack propagation in homogeneous, isotropic solids (Rosakis et al., 1999, 2000), in bimaterials (Lambros and Rosakis, 1995; Singh et al., 1997; Rosakis et al., 1998) and in transversely isotropic solids (Coker and Rosakis, 2001) all of which feature special directions of inhomogeneity in fracture toughness (i.e., planes of reduced fracture toughness). Gao et al. (1999) made an interesting comparison of intersonic cracks with intersonic glide edge dislocations and developed a unified treatment for investigating the existence of radiation-free intersonic speeds for either system. Huang et al. (1999) derived the asymptotic fields around an intersonically propagating mode II crack in a transversely isotropic material. They showed that a radiation-free intersonic speed exists for a mode II crack in a transversely isotropic solid, similar to $\sqrt{2}c_s$ for the homogeneous case, where the crack tip dynamic energy release rate is finite. Yu and Suo (2000) developed a unified method based on analytic function theory to obtain the near-tip fields for a quasi-static/subsonic/intersonic crack in a homogeneous solid or along a bimaterial interface with the constituents being either isotropic or anisotropic. They used a Dugdale-type cohesive zone model and identified those crack speed regimes that result in negative cohesive zone length to be forbidden.

Needleman (1999) performed a finite element simulation of the intersonic shear crack experiments of Rosakis et al. (1999) using a cohesive surface constitutive relation for the weak crack path. He found that a shear crack initiating from a pre-crack along the weak path either propagates at c_R or accelerates to a near constant intersonic speed above $\sqrt{2}c_s$. He examined the effect of shear strength of the interface, the fracture energy and the duration of the loading pulse on the transition from a subRayleigh to an intersonic speed, as well as on the terminal speed achieved. Abraham and Gao (2000) performed an atomistic simulation of shear crack propagation along a weak interface characterized by a Lennard–Jones potential, joining two harmonic crystals. Their simulations showed that a shear dominated crack, soon after initiation accelerates to c_R and then nucleates an intersonic daughter crack that travels at c_l, in accordance with the predictions of Burridge (1973) and Andrews (1976). When the applied strain was completely relaxed after the initiation of the daughter crack, they found shear crack propagation at $\sqrt{2}c_s$, similar to the behavior observed in the experiments of Rosakis et al. (1999). Geubelle and Kubair (2001) studied numerically, using a spectral boundary element scheme, the problem of transient initiation and propagation of a mixed mode in-plane crack in its own plane under the action of remote uniform mixed mode loading. Using a quasi-linear cohesive failure model, they observed that a shear dominated crack can attain intersonic speeds either by initiation of a secondary slip zone in front of the tip (the Burridge–Andrews mechanism) or simply by a rapid, but smooth acceleration through the forbidden regime. The latter case, which was also observed by Johnson (1990) is in contradiction with the theoretical prediction that an in-plane crack with a continuously varying speed cannot accelerate through c_R. During steady-state intersonic crack growth, it was found that the cohesive failure was entirely by shear even under

far-field mixed mode loading, consistent with analytical predictions. Gao et al. (2001) studied the transition of a subsonic mode II crack to intersonic speeds using a cohesive fracture criterion and showed that the predictions of continuum elasticity theories are captured very well by atomistic simulations. More recently Huang and Gao (2001) obtained the fundamental solution for the intersonic shear crack problem, which may be used for obtaining the general solutions for intersonic mode II cracks under arbitrary initial equilibrium fields.

Our current work aims at adding to the substantial body of knowledge on dynamic mode II crack growth. In particular, the work is motivated by the experimental observations of intersonic shear cracks in our laboratory. In the next section, a brief description is provided of the specimen configuration, experimental setup, the conditions for attaining straight-ahead intersonic crack growth, observed crack speed histories and the recorded isochromatic fringe patterns around an intersonically propagating mode II crack. Also the singular solution of Freund (1979) for intersonic mode II cracks is revisited and its predictions are examined in light of the experimental observations, motivating the necessity of a cohesive zone model. In Sections 3–5, a rate-dependent cohesive zone model for steady-state dynamic mode II crack propagation is proposed and analyzed, wherein the cohesive shear traction varies linearly with the local sliding rate. The governing equations are solved using a standard technique in analytic function theory and the nature of the predicted near-tip fields is examined. In Section 6, a propagation criterion is imposed, which requires a constant crack tip sliding displacement, and its predictions on the fracture energy, cohesive zone length, crack stability and isochromatic fringe patterns are discussed and compared with the experimental observations as well as with known analytical and numerical results from the literature. Finally comments are made on the validity of the proposed model.

2. Experimental observations of intersonic mode II crack growth

Experiments were performed in the laboratory to verify the possibility of intersonic mode II crack growth in a constitutively homogeneous, isotropic, linear elastic solid. To ensure the directional stability of a propagating mode II crack, a thin layer of lower fracture toughness, compared to that of the monolithic material, was introduced along the prospective crack path. The specimens were made by bonding two identical plates ($6'' \times 5''$) of Homalite-100, a brittle polyester resin, as shown in the inset of Fig. 1. The thickness of the plates was either $3/16''$ or $1/4''$ or $3/8''$. Homalite-100 exhibits the property of stress-induced birefringence, enabling the use of dynamic photoelasticity for visualizing the stress state in the specimen. The bonding process was chosen carefully so that the constitutive properties of the bond are close to those of the bulk material. A polyester resin solution (99.5% by wt) was used for bonding, with methyl ethyl ketone peroxide as hardener (0.4%) and cobalt octate (0.1%) as catalyst. The bond was cured for 48 h at room temperature. The thickness of the bond was approximately 20–30 μm. A notch, 25 mm long and 2 mm wide was machined on the upper half of the specimen along the bond line (see Fig. 1). The relevant material properties of Homalite at strain rates of the order 10^3 s^{-1} are : shear modulus, $\mu = 1.9$ GPa, Poisson's ratio, $\nu = 0.34$, c_R

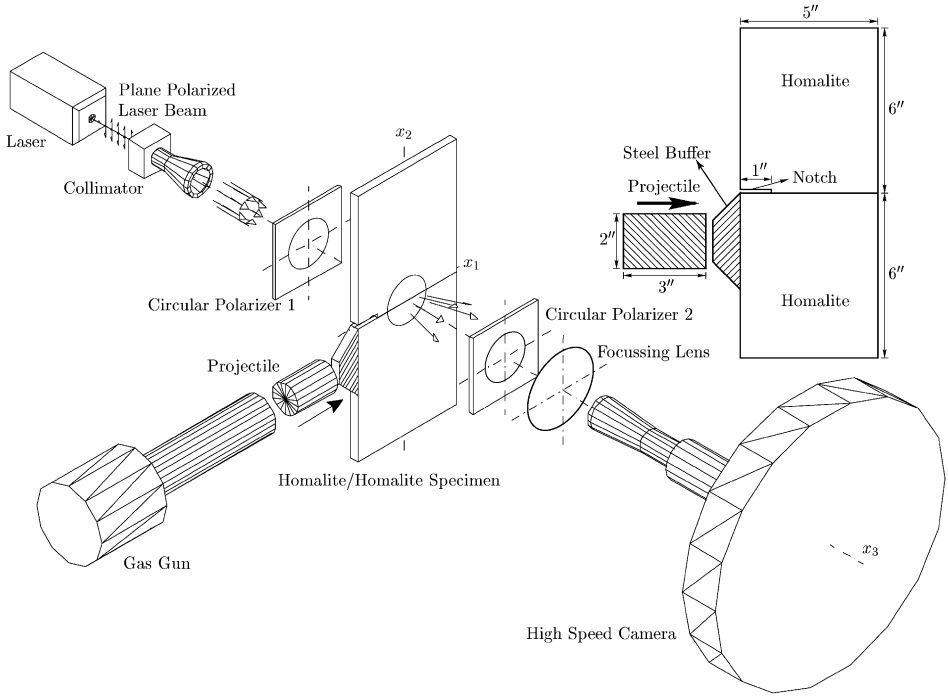

Fig. 1. Dynamic photoelasticity setup showing a Homalite/Homalite specimen placed inside a circular polariscope and being subjected to impact shear loading by a projectile fired from a high-speed gas gun. The resulting isochromatic fringe patterns are recorded by high-speed photography. The specimen geometry is shown in the inset.

(plane stress) $=1155$ m/s, $c_s = 1255$ m/s and c_l (plane stress) $= 2187$ m/s. The tensile strength of bulk Homalite is about 35 MPa and the shear strength of the bond τ_0, as measured using a conventional Iosipescu shear test fixture is around 12–16 MPa.

The experimental setup used to investigate dynamic crack growth under impact shear loading is shown in Fig. 1. Dynamic photoelasticity was chosen for capturing the stress field near the propagating crack tip because of its ability to visualize shear Mach waves, anticipated by the intersonic crack solutions. The specimen was subjected to asymmetric impact loading with a cylindrical projectile fired from a high-speed gas gun. The projectile was 3″ long, 2″ in diameter and was made of hardened steel. Compressed air at 12–80 psi was used as the driving medium, which resulted in projectile velocities ranging from 8 to 40 m/s. A steel buffer was bonded to the speciment at the impact site to prevent shattering and to induce a planar loading wave front. The compressive longitudinal wave loads the notch, initially, in a predominantly shear mode (Lee and Freund, 1990). A notch was preferred to be the crack initiation site instead of a pre-crack, so that the transmission of stress waves into the top half is prevented, thus ensuring that the notch tip is loaded under predominantly mode II conditions. The dynamic stress field produced by the impact loading was recorded using photoelasticity in conjunction

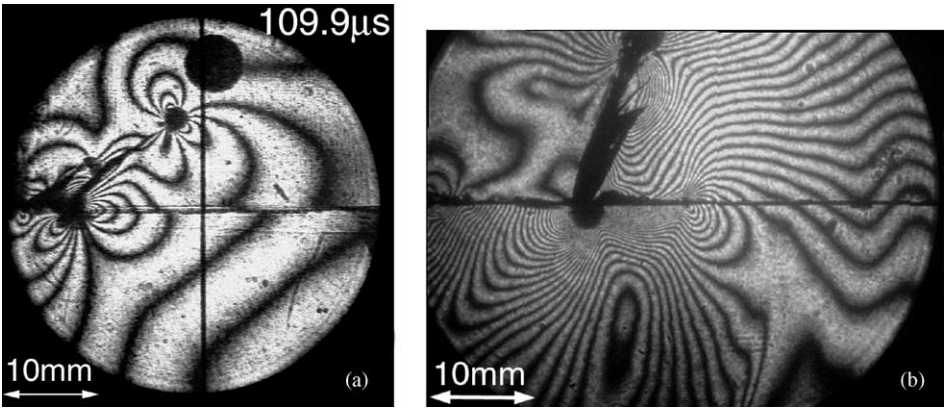

Fig. 2. Single edge notch/crack along a weak plane in Homalite under impact shear loading: (a) Impact speed = 11 m/s. A crack initiating from the notch kinks at 39° to the weak plane. (b) Impact speed = 20 m/s. The pre-crack kinks at 70° to the weak plane. In addition a second crack is also seen propagating along the weak plane.

with high-speed photography. Photoelasticity is a common optical technique used in solid mechanics applications which provides real-time full field information about the stress state and the reader is referred to Dally and Riley (1991) for further details. The isochromatic fringe pattern was recorded by a rotating mirror-type high-speed camera capable of recording 80 frames at framing rates up to 2 million frames per second.

Fig. 2 shows the effect of projectile impact speed on crack initiation from the tip of the notch/pre-crack in the specimen. Fig. 2(a) shows the isochromatic fringe pattern around the notch at 109.9 μs (measured from time of impact), for a projectile impact speed of 11 m/s. Around 50 μs after impact, a kinked crack was observed to initiate from the notch, inclined at an angle of 39° to the weak plane ahead. If we assume, that the kink angle observed follows the criterion of maximal energy dissipation (Hutchinson and Suo, 1992), it can be deduced that the mode mixity $\psi = \tan^{-1}(K_{II}/K_I)$ at initiation is $\approx 24^\circ$. Hence, at initiation, the magnitude of the mode I stress intensity factor, K_I was almost 2.25 times that of the mode II stress intensity factor, K_{II}. The opening dominated nature of the notch-tip fields can also be readily expected from the time taken for crack initiation after impact. Crack initiation occurs around 50 μs, by which time unloading waves due to the finite width of the loading pulse (≈ 28 μs), reflections from the far end (with respect to the notch tip) of the buffer plate and also from the free surface to the left on the top half of the specimen, have arrived and impinged on the notch eventually changing its mode mixity to a predominantly opening mode. The kinked crack propagates with mode I symmetry at its tip, as seen from the symmetry of the two lobes oriented at 90° to the crack plane. The average speed of the kinked crack was $\approx 0.26c_s$. Fig. 2(b) shows the isochromatic fringe pattern around the pre-crack in a specimen subjected to projectile impact at 20 m/s. A kinked crack is observed to initiate from the loaded pre-crack at an angle of 70° to the crack plane. Again using the criterion of maximal energy dissipation, one can see that at initiation, mode mixity

$\psi \approx 72^{\circ}$. Hence, at initiation, magnitude of K_{II} was almost 3.1 times that of K_I. Apart from the kinked crack, another crack can also be observed to propagate straight ahead, along the weak plane (see Fig. 2(b)). The crack along the weak plane is likely to be shear dominated, since it initiated from a shear dominated pre-crack, though the isochromatic fringe pattern is complicated by the presence of the kinked crack. Also the shear crack along the weak plane propagates at a substantially higher speed compared to the kinked crack. Schardin (1959) also reported a similar phenomenon, where a crack along a pre-existing scratch on a glass plate travels at a higher speed as compared to a crack in solid glass. This suggests that a higher impact speed resulting in initiation under predominantly shearing mode might result in a fast shear crack propagating ahead along the weak plane. Also, if the fracture energy of the weak plane is low compared to the monolithic material then the kinked crack might be eliminated. The substantial increase in the number of fringes observed is a reflection of the fact that the impact speed was higher and also due to the fact that the specimen thickness in the higher impact case was $3/8''$, where as the specimen thickness in the lower impact case was $1/4''$. Once a straight-ahead shear crack is initiated, and its directional stability is maintained, it is possible for it to achieve intersonic speeds as shown in Fig. 3.

Fig. 3(a) shows a selected isochromatic fringe pattern around a propagating mode II crack along the weak plane. At initiation, the notch is subjected to a mixed mode loading with a negative K_I and a negative K_{II} (Lee and Freund, 1990; Mason et al., 1992). After initiation, however, the nature of the crack tip deformation must be pure mode II. To sustain the expected negative K_I at the propagating sharp crack tip, the crack faces must come closer from their initial configuration. A negative K_I is possible at the tip of a notch, where the notch faces are separated by a finite notch width, however for a sharp crack, the crack faces are already in contact (but traction free) in their rest configuration. Hence, a sharp crack tip cannot sustain a negative K_I, and pure mode II conditions must prevail at the tip, albeit with negative normal tractions acting on the crack faces (which annul the negative K_I required at the tip due to the mixity of far-field loading). The field of view shown in Fig. 3(a) has a diameter of 50 mm and is centered on the weak plane, 38.2 mm ahead of the notch tip. Impact speed of the projectile was 20.8 m/s. The time after impact as well as the crack tip speed is shown in the figure. The crack speed is in the intersonic range. We can clearly distinguish two lines radiating from the crack tip, across which the fringe pattern changes abruptly (lines of stress field discontinuity). These two lines correspond to the two traveling shear Mach waves, which limit the spread of shear waves emanating from the crack tip as it propagates along the interface at intersonic speeds. The angle ξ the Mach waves make with the crack faces is related to the crack speed through

$$\xi = \sin^{-1}(c_s/v). \tag{1}$$

Our experimental observations on intersonic mode II crack growth have been reported in greater detail in Rosakis et al. (1999, 2000).

Fig. 3(b) shows the variation of crack speed as the shear crack propagates along the weak plane. Crack length includes length of the initial notch which was about $1''$. Data is shown for two similar experiments, varying in the position of the field of view. Experiment 9 corresponds to a projectile impact speed of 26.8 m/s and the field

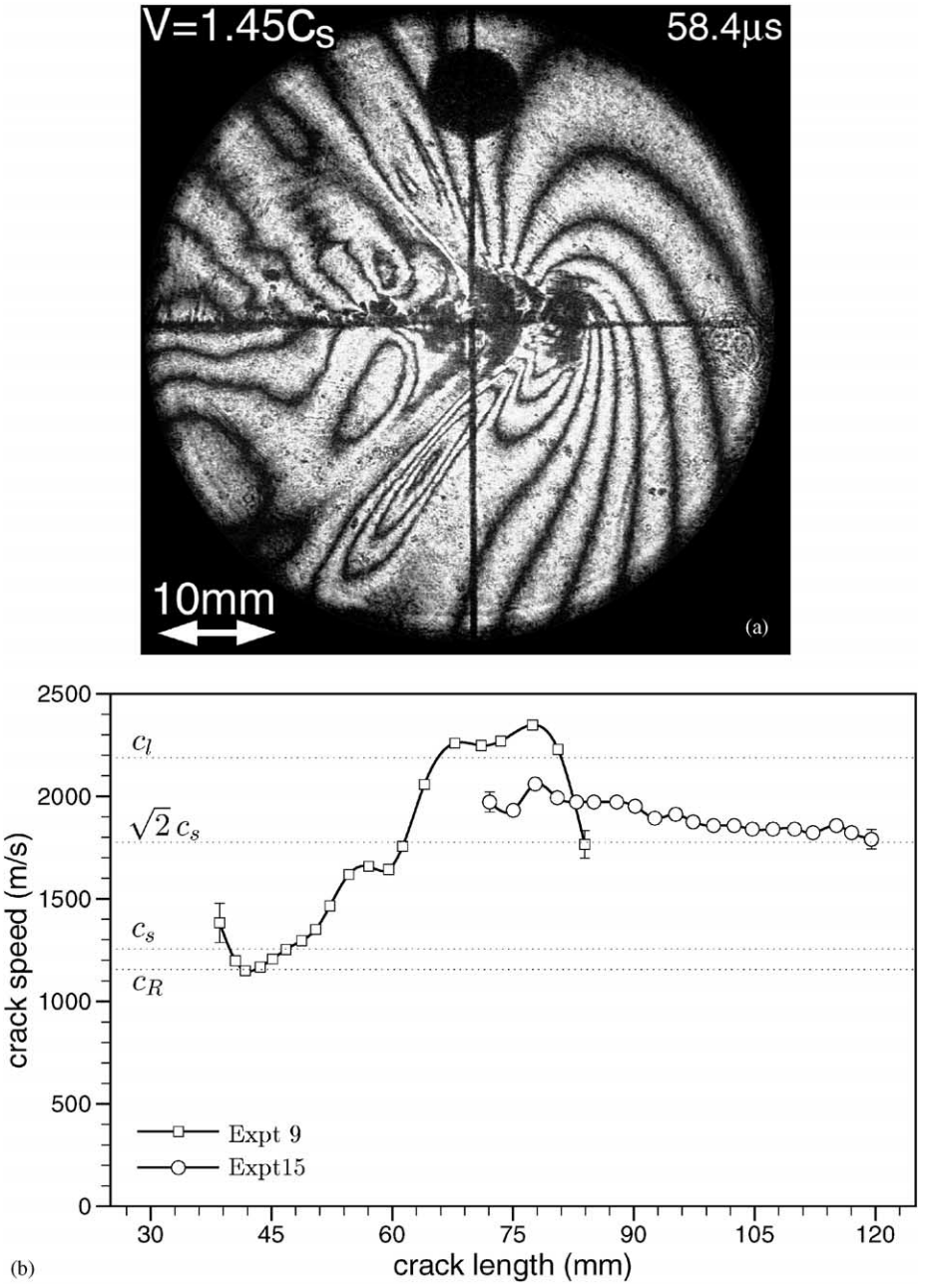

Fig. 3. (a) Isochromatic fringe pattern around a propagating intersonic crack along a weak plane in Homalite. (b) Evolution of crack speed as the crack propagates along the weak plane. Expt 9 corresponds to an impact speed of 26.8 m/s and the field of view of 50 mm was centered at 29.1 mm ahead of the notch tip. Crack speed data was obtained from crack length history. Expt 15 corresponds to an impact speed of 27.7 m/s and the field of view of 50 mm was centered at 63.1 mm ahead of the notch tip. Crack speed data was obtained from Mach angle measurements.

of view of 50 mm was centered on the weak plane, 29.1 mm ahead of the notch tip. Crack speed data shown for this experiment was obtained from crack length history. A second-order interpolating polynomial is obtained for every three successive points in the crack length history, which is then differentiated to give the crack speed for the mid-point. Experiment 15 corresponds to an impact speed of 27.7 m/s and the field of view of 50 mm was centered on the weak plane, 63.1 mm ahead of the notch tip. The crack speed data shown for this experiment was obtained by measuring the Mach angle and using the relation (1). Crack speed estimates from Mach angle measurements are more accurate compared to those obtained from the crack length history due to the inherent propagation of errors in the differentiation process. In the case of Experiment 9, the crack had just initiated and the Mach waves had not been radiated over a sufficient distance to be clearly distinguished. Hence we had to resort to measuring the crack speed from crack length history.

From Fig. 3(b) we see that the initially recorded crack tip speed is close to the shear wave speed of Homalite (within experimental error of ± 100 m/s) beyond which it accelerates (at the order of 10^8 m/s^2), thus becoming intersonic. Thereafter, it continues to accelerate up to the plane stress longitudinal wave speed of Homalite, following which it decelerates and ultimately reaches a steady-state value close to $\sqrt{2}c_s$. It should be recalled here that the speed regime between c_R and c_s is forbidden by theory, based on energy considerations. For this speed regime, the asymptotic singular solution predicts radiation of energy away from the crack tip (negative energy release rate), which is not possible on physical grounds. The non-singular solution predicts zero energy flux to the tip, which is also inadmissible since crack propagation requires finite energy dissipation in the tip region. Hence a crack with a smoothly varying crack speed cannot pass through this forbidden regime. According to this rationale, a crack will have to jump discontinuously from the subRayleigh regime to the intersonic regime. However, another possibility for generating such intersonic speeds is to bypass this forbidden regime by nucleating a crack from the initial notch that instantaneously starts to propagate at a speed above c_s. Within our experimental time resolution the second scenario seems to be the most probable.

The singular near-tip fields for an intersonic mode II crack were obtained by Freund (1979). A comparison of our experimentally recorded isochromatic fringe patterns with those predicted by the Freund's singular solution was reported in Rosakis et al. (1999, 2000). This comparison, although very favorable on many grounds, eventually serves to motivate the use of cohesive zone models in the analysis of intersonic fracture. Freund's singular solution predicts that the crack tip stress singularity q for an intersonic mode II crack is a function of crack speed. It is found that q increases monotonically from 0 at c_s to $\frac{1}{2}$ at $\sqrt{2}c_s$ and thereafter decreases monotonically to 0 at c_l. An implication of this behavior of q is that the dynamic energy release rate G, defined as the energy flux into the crack tip per unit crack advance per unit length along the crack front, is zero every where in the intersonic regime except at $\sqrt{2}c_s$ where it has a finite value.

For intersonic mode II cracks, the idealization of the crack tip process zone to a point-size dissipative region results in a physically unrealistic situation, wherein the requirement of a positive energy flux to the crack tip region is met only at $\sqrt{2}c_s$. On the contrary, the experimental observations show crack growth at all intersonic speeds

(see Fig. 3(b)). Andrews (1976) pointed out that for intersonic cracks, where the crack tip stress singularity is less than 1/2, a non-zero fracture energy is supported only for the case where the stress drop is not abrupt, i.e., the crack tip region must have a finite extent. A comparatively simple way to eliminate this difficulty would be to incorporate a dissipative zone of finite size in front of the tip (Andrews, 1976; Broberg, 1989). In such a case, they showed that positive energy flux to the dissipative zone results at all intersonic speeds except at c_s and c_l. A dissipative zone of finite extent can be incorporated readily by considering a line cohesive zone of finite extent in front of the tip.

Compared to the experimental results reported in Rosakis et al. (1999), we find that when the impact speed is lower and the field of view is much closer to the initiation site (see Fig. 3(a)), then the Mach waves radiating from the tip are no longer very sharp and have structure with a finite width. The finite width of the Mach waves is not modeled by the singular solution, which predicts line Mach waves, along which the stress components are singular with the same order of singularity as at the crack tip. An intersonic mode II crack model incorporating a cohesive zone of finite extent is required to model the structure of the Mach waves as well as the crack tip process zone.

In the current paper, steady-state subsonic and intersonic mode II crack propagation with a rate-dependent cohesive zone is analyzed. A line cohesive zone is introduced in front of the crack tip, with the tractions on the cohesive surfaces depending linearly on the local sliding rate. Such a line cohesive zone has a natural motivation from the experiments described above, where the fracture process zone was mostly confined to a thin weak layer (the bond line) in front of the crack tip. The experiments were also conducted with a strongly rate-dependent constituents and bonds and hence a fast increase in shear stress within the fracture process zone may result in a substantial increase (or, perhaps in some cases decrease) in the cohesive shear strength of the material, motivating a cohesive law that takes rate effects into account. Data on the dependence of cohesive traction on sliding rate at the rates experienced during the experiments is rather obscure. However, in this paper we limit ourselves to those cases where the shear strength increases with sliding rate.

3. Propagating mode II crack with a line cohesive zone

Consider a semi-infinite mode II crack with a line cohesive zone of length L in front of the tip, propagating at a constant speed v through a homogeneous, isotropic, linear elastic medium under 2D plane strain or plane stress conditions (see Fig. 4(a)). The crack is constrained to propagate in its own plane (a situation that simulates the existence of a zone of lower toughness or a preferable crack path) and the crack speed can be either subsonic or intersonic ($0 < v < c_l$). For planar deformation, the displacement field u_α with respect to a fixed coordinate system (x_1, x_2) can be expressed in terms of two displacement potentials $\phi(x_1, x_2, t)$ and $\psi(x_1, x_2, t)$ as

$$u_\alpha(x_1, x_2, t) = \phi_{,\alpha}(x_1, x_2, t) + \varepsilon_{\alpha\beta}\psi_{,\beta}(x_1, x_2, t), \tag{2}$$

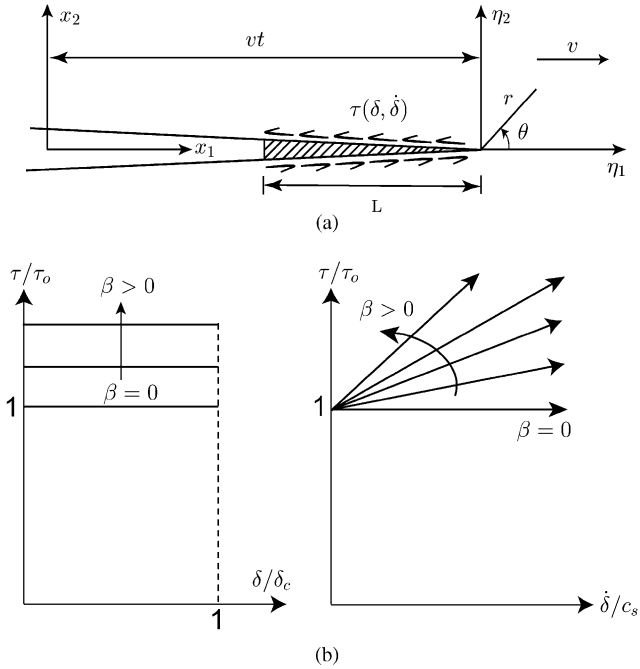

Fig. 4. Dynamic mode II crack in a homogeneous, isotropic, linear elastic solid with a rate-dependent line cohesive zone: (a) illustration showing the cohesive zone and the crack tip coordinate system; (b) rate-dependent cohesive law relating the shear traction to the local sliding displacement and the local sliding rate.

where $\varepsilon_{\alpha\beta}$ is the 2D alternator with $\varepsilon_{11}=\varepsilon_{22}=0$ and $\varepsilon_{12}=-\varepsilon_{21}=1$. The usual cartesian index notation is employed, wherein repeated indices imply summation. Greek indices take the values 1 & 2 and roman indices take the values 1, 2 & 3. Also $(\cdot)_{,\alpha}=\partial(\cdot)/\partial x_\alpha$ and an overdot on any field quantity represents derivative with respect to time.

The strain field and stress field components can be expressed in terms of these displacement potentials using the strain–displacement relations and the generalized Hooke's law. By introducing a moving coordinate system $(\eta_1,\eta_2)=(x_1-vt,x_2)$ centered at the front end of the cohesive zone (see Fig. 4(a)), and assuming that crack growth is steady state, one finds that the equations of motion in terms of ϕ and ψ reduce to (Freund, 1990; Broberg, 1999a)

$$\phi_{,11}(\eta_1,\eta_2)+\frac{1}{\alpha_l^2}\phi_{,22}(\eta_1,\eta_2)=0,\quad 0<v<c_l, \tag{3a}$$

$$\psi_{,11}(\eta_1,\eta_2)+\frac{1}{\alpha_s^2}\psi_{,22}(\eta_1,\eta_2)=0,\quad 0<v<c_s, \tag{3b}$$

$$\psi_{,11}(\eta_1,\eta_2)-\frac{1}{\alpha_s^2}\psi_{,22}(\eta_1,\eta_2)=0,\quad c_s<v<c_l, \tag{3c}$$

where

$$\alpha_l = \sqrt{\left[1 - \frac{v^2}{c_l^2}\right]}, \quad \alpha_s = \sqrt{\left[1 - \frac{v^2}{c_s^2}\right]} \quad \text{and} \quad \hat{\alpha}_s = \sqrt{\left[\frac{v^2}{c_s^{2-1}} - 1\right]}. \tag{4}$$

Thus the motion is governed by two elliptic equations in the subsonic case, whereas for the intersonic case it is governed by an elliptic and a hyperbolic equation. Henceforth, the formulations for subsonic and intersonic cases are treated separately.

3.1. *Subsonic case,* $0 \leqslant v < c_s$

The most general solutions for the displacement potentials are given by (Freund, 1990)

$$\phi(\eta_1, \eta_2) = \mathrm{Re}\{F(z_l)\}, \tag{5a}$$

$$\psi(\eta_1, \eta_2) = \mathrm{Im}\{G(z_s)\}, \tag{5b}$$

where $F(\cdot)$ is a function, analytic with respect to its argument, $z_l = \eta_1 + \mathrm{i}\alpha_l\eta_2$ everywhere in the z_l-plane except on the crack faces and $G(\cdot)$ is a function, analytic with respect to its argument, $z_s = \eta_1 + \mathrm{i}\alpha_s\eta_2$ everywhere in the z_s-plane except on the crack faces. The stress and displacement fields may now be expressed in terms of the unknown functions F and G.

For a mode II crack, the displacement component u_1 is anti-symmetric with respect to the crack plane, where as the component u_2 is symmetric with respect to the crack plane. Hence

$$F'^{-}(\eta_1) = -\bar{F}'^{-}(\eta_1), \tag{6a}$$

$$G'^{-}(\eta_1) = -\bar{G}'^{-}(\eta_1). \tag{6b}$$

The superscripts "+" and "−" stand for the limits $\eta_2 \to 0^+$ and $\eta_2 \to 0^-$, respectively. The traction boundary conditions on the cohesive surfaces and the crack faces are given by

$$\sigma_{22}^{\pm}(\eta_1) = 0, \quad \eta_1 < 0, \tag{7a}$$

$$\sigma_{12}^{\pm}(\eta_1) = \begin{cases} \tau(\eta_1/L), & -L < \eta_1 < 0, \\ 0, & \eta_1 < L, \end{cases} \tag{7b}$$

where $\tau(\eta_1/L)$ is the unknown cohesive traction distribution on the cohesive surfaces. Substituting for the stress fields in terms of F and G and incorporating the mode II symmetries from (6), we have

$$(1 + \alpha_s^2)\{F''^{+}(\eta_1) - F''^{-}(\eta_1)\} + 2\alpha_s\{G''^{+}(\eta_1) - G''^{-}(\eta_1)\} = 0, \quad \eta_1 < 0, \tag{8a}$$

$$\mathrm{i}\mu\left[\alpha_l\{F''^{+}(\eta_1) + F''^{-}(\eta_1)\} + \frac{(1 + \alpha_s^2)}{2}\{G''^{+}(\eta_1) + G''^{-}(\eta_1)\}\right] = \begin{cases} \tau(\eta_1/L), & -L < \eta_1 < 0, \\ 0, & \eta_1 < -L. \end{cases} \tag{8b}$$

The first of the two equations above implies that the function

$$P(z) = (1 + \alpha_s^2)F''(z) + 2\alpha_s G''(z), \tag{9}$$

which is analytic everywhere in the $z = \eta_1 + i\eta_2$ plane, except possibly along the crack line, is continuous across the crack line and it does not have any poles there. Hence $P(z)$ is an entire function. Furthermore, the vanishing of stress at remote points implies that $P(z) \to 0$ as $|z| \to \infty$. Hence $P(z)$ is a bounded entire function and by Liouville's theorem $P(z)$ is a constant. In particular, $P(z) = 0$ everywhere. Hence

$$G''(z) = \frac{-(1 + \alpha_s^2)}{2\alpha_s} F''(z). \tag{10}$$

The second equation in (8) becomes

$$iF''^{+}(\eta_1) - (-i)F''^{-}(\eta_1) = \begin{cases} \dfrac{4\alpha_s}{\mu R(v)}\tau(\eta_1/L), & -L < \eta_1 < 0, \\ 0, & \eta_1 < -L, \end{cases} \tag{11}$$

where $R(v) = 4\alpha_1\alpha_s - (1 + \alpha_s^2)^2$ is the Rayleigh function. This is an inhomogeneous Hilbert problem. The general solution of (11), considering only the singular terms, is given by (Muskhelishvili, 1963; Gakhov, 1990)

$$F''(z) = \frac{A_0}{\sqrt{z}} + \frac{1}{2\pi i}\frac{4\alpha_s}{\mu R(v)}\frac{1}{\sqrt{z}}\int_{-L}^{0} \frac{\sqrt{|\xi|}\tau(\xi/L)}{\xi - z}\,d\xi. \tag{12}$$

Following (6) we can readily conclude that A_0 is pure imaginary.

The shear stress ahead of the crack tip is given by

$$\sigma_{12}(\eta_1 > 0, \eta_2 = 0) = \frac{i\mu R(v)}{2\alpha_s}\left\{\frac{A_0}{\sqrt{|\eta_1|}} + \frac{1}{i\pi}\frac{2\alpha_s}{\mu R(v)}\frac{1}{\sqrt{|\eta_1|}}\int_{-L}^{0}\frac{\sqrt{|\xi|}\tau(\xi/L)}{\xi - |\eta_1|}\,d\xi\right\}. \tag{13}$$

Far ahead of the crack tip, i.e., for $\eta_1 = D \gg L$, $\eta_2 = 0$, the solution must match the square root singular stress intensity factor field for steady subsonic crack growth.

$$\sigma_{12}(\eta_1 = D, \eta_2 = 0) \approx \frac{\mu R(v)}{2\alpha_s}\frac{iA_0}{\sqrt{D}} = \frac{K_{II}^{d}}{\sqrt{2\pi D}}.$$

$$\Rightarrow iA_0 = \frac{1}{\sqrt{2\pi}}\frac{K_{II}^{d}}{\mu}\frac{2\alpha_s}{R(v)}. \tag{14}$$

Also, with the presence of a cohesive zone, the stresses must be bounded at its front end and the stress intensity factor here should vanish.

$$\lim_{\eta_1 \to 0^+} \sigma_{12}(\eta_1 > 0, \eta_2 = 0)\sqrt{2\pi\eta_1} = 0$$

$$\Rightarrow iA_0 = \frac{1}{\mu\pi}\frac{2\alpha_s}{R(v)}\int_{-L}^{0}\frac{\tau(\xi/L)}{\sqrt{|\xi|}}\,d\xi \tag{15}$$

$$\Rightarrow K_{\mathrm{II}}^{\mathrm{d}} = \sqrt{\frac{2}{\pi}} \int_{-L}^{0} \frac{\tau(\xi/L)}{\sqrt{|\xi|}}\, \mathrm{d}\xi. \tag{16}$$

The η_1-gradient of the sliding displacement u_1 along the upper cohesive surface is given by

$$u_{1,1}(-L < \eta_1 < 0, \eta_2 \to 0^+) = -\frac{v^2}{c_{\mathrm{s}}^2} \frac{\alpha_{\mathrm{s}}}{R(v)} \frac{\sqrt{|\eta_1|}}{\mu\pi}\ \mathrm{pv} \int_{-L}^{0} \frac{\tau(\xi/L)}{\sqrt{|\xi|}(\xi + |\eta_1|)}\, \mathrm{d}\xi. \tag{17}$$

For steady crack growth $\dot{(\cdot)} = -v(\cdot)_{,1}$. Hence the above result relates the rate of sliding within the cohesive zone to the cohesive traction resisting the sliding.

3.2. Intersonic case, $c_{\mathrm{s}} < v < c_{\mathrm{l}}$

Owing to the symmetry of the problem, we consider the solution to equations (3) only in the upper half-plane ($\eta_2 \geqslant 0$). The general solutions for the displacement potentials are (Freund, 1990)

$$\phi(\eta_1, \eta_2) = \mathrm{Re}\{F(z_{\mathrm{l}})\}, \tag{18a}$$

$$\psi(\eta_1, \eta_2) = g(\eta_1 + \hat{\alpha}_{\mathrm{s}}\eta_2), \tag{18b}$$

where F is the same function as in the subsonic case and $g(\cdot)$ is a real function of its argument. The radiation condition is employed here, i.e., an intersonic crack is only capable of generating backward running shear waves (Freund, 1979; Liu et al., 1995). The displacement and stress fields may now be expressed in terms of the unknown functions, F and g.

Mode II symmetries, ahead of the crack tip reduce to

$$F''^{+}(\eta_1) = -\bar{F}''^{-}(\eta_1), \quad \eta_1 > 0, \tag{19a}$$

$$g''^{+}(\eta_1) = 0, \quad \eta_1 > 0. \tag{19b}$$

Following (19) we can define $\theta(z)$ (by analytic continuation), a function analytic everywhere on the complex z-plane except on the crack faces as

$$\theta(z) = \begin{cases} F''(z), & \mathrm{Im}\{z\} \geqslant 0, \\ -\bar{F}''(z), & \mathrm{Im}\{z\} < 0. \end{cases} \tag{20}$$

The traction boundary conditions on the upper crack face and the cohesive surface reduce to

$$g''^{+}(\eta_1) = \frac{-(1 - \hat{\alpha}_{\mathrm{s}}^2)}{4\hat{\alpha}_{\mathrm{s}}} \{F''^{+}(\eta_1) + \bar{F}''^{-}(\eta_1)\}, \quad \eta_1 < 0, \tag{21a}$$

$$\mu[-2\alpha_{\mathrm{l}}\, \mathrm{Im}\{F''^{+}(\eta_1)\} - (1 - \hat{\alpha}_{\mathrm{s}}^2) g''^{+}(\eta_1)] = \begin{cases} \tau(\eta_1/L), & -L < \eta_1 < 0, \\ 0, & \eta_1 < -L. \end{cases} \tag{21b}$$

The second of the above equations reduces to

$$[(1-\hat{\alpha}_s^2)^2+4i\alpha_1\hat{\alpha}_s]\theta^+(\eta_1)-[(1-\hat{\alpha}_s^2)^2-4i\alpha_1\hat{\alpha}_s]\theta^-(\eta_1)$$

$$=\begin{cases}\dfrac{4\hat{\alpha}_s}{\mu}\tau(\eta_1/L), & -L<\eta_1<0,\\ 0, & \eta_1<-L.\end{cases} \tag{22}$$

Similar to the subsonic case, the general solution for the inhomogeneous Hilbert problem in the upper half-plane ($\eta_2 \geqslant 0$), is given by

$$\theta(z)=F''(z)=\frac{A_0}{z^q}+\frac{1}{2\pi i}\frac{4\hat{\alpha}_s}{\mu R_q}\frac{1}{z^q}\int_{-L}^{0}\frac{|\xi|^q\tau(\xi/L)}{\xi-z}\,d\xi, \tag{23}$$

where

$$q=\frac{1}{\pi}\tan^{-1}\left[\frac{4\alpha_1\hat{\alpha}_s}{(1-\hat{\alpha}_s^2)^2}\right], \tag{24a}$$

$$R_q=\sqrt{16\alpha_1^2\hat{\alpha}_s^2+(1-\hat{\alpha}_s^2)^4}. \tag{24b}$$

From mode II symmetries we can readily conclude that A_0 is pure imaginary.

The shear stress ahead of the crack tip is given by

$$\sigma_{12}(\eta_1>0,\eta_2=0)=\frac{2\mu\alpha_1 iA_0}{|\eta_1|^q}+\frac{\sin q\pi}{\pi}\frac{1}{|\eta_1|^q}\int_{-L}^{0}\frac{|\xi|^q\tau(\xi/L)}{\xi-|\eta_1|}\,d\xi. \tag{25}$$

Far ahead of the crack tip, i.e., for $\eta_1=D\gg L$, $\eta_2=0$, the solution must match the singular solution.

$$\sigma_{12}(\eta_1=D,\eta_2=0)\approx\frac{2\mu\alpha_1 iA_0}{D^q}=\frac{K_{II}^{*d}}{\sqrt{2\pi}D^q}.$$

$$\Rightarrow iA_0=\frac{1}{\sqrt{2\pi}}\frac{K_{II}^{*d}}{2\mu\alpha_1}. \tag{26}$$

K_{II}^{*d} is the intersonic mode II stress intensity factor. Also, with the presence of a cohesive zone, the stresses must be bounded at the front end and the stress intensity factor here should vanish.

$$\lim_{\eta_1\to 0^+}\sigma_{12}(\eta_1>0,\eta_2=0)\sqrt{2\pi}\eta_1^q=0$$

$$\Rightarrow iA_0=\frac{1}{2\mu\alpha_1}\frac{\sin q\pi}{\pi}\int_{-L}^{0}\frac{\tau(\xi/L)}{|\xi|^{1-q}}\,d\xi \tag{27}$$

$$\Rightarrow K_{II}^{*d}=\sin q\pi\sqrt{\frac{2}{\pi}}\int_{-L}^{0}\frac{\tau(\xi/L)}{|\xi|^{1-q}}\,d\xi. \tag{28}$$

The relation between the rate of sliding within the cohesive zone and the cohesive shear traction resisting the sliding is given by

$$u_{1,1}(-L<\eta_1<0,\eta_2\to 0^+)=\frac{(1+\hat{\alpha}_s^2)\sin^2 q\pi}{4\pi\mu\alpha_1}$$

$$\times\left\{\frac{\pi\tau(\eta_1/L)}{\tan q\pi}-|\eta_1|^{1-q}\,\mathrm{pv}\int_{-L}^{0}\frac{\tau(\xi/L)}{|\xi|^{1-q}(\xi+|\eta_1|)}\,d\xi\right\}. \tag{29}$$

4. Rate-dependent cohesive law

Rate-dependent cohesive constitutive relations, which relate the traction on a cohesive surface to the local displacement rate, have been used in the past for modeling elastic–viscoplastic material behavior (Glennie, 1971a,b; Freund and Lee, 1990). Glennie (1971a) analyzed the problem of a uniformly moving semi-infinite mode I crack in plane strain, with a rate-dependent cohesive zone in front of it. He used a strip yield zone, with the yield stress linearly dependent on strain rate to model thin plastic zones ahead of running mode I cracks in sheets of mild-steel. He suggested that the increased resistance to plastic flow at high crack speeds can explain the relatively low terminal speeds observed for running mode I cracks. Freund and Lee (1990) analyzed the same problem, and to model the failure mode transition observed in some ferritic steels, introduced two different fracture criteria, one for ductile fracture based on a critical crack tip opening displacement and another for brittle fracture based on a critical stress in front of the tip. They investigated the dependence of the far-field applied stress intensity factor, crack speed and a rate parameter on the failure mode selection.

The rate-dependent cohesive law used here is similar to the one used by Glennie (1971a,b) and Freund and Lee (1990). The cohesive constitutive relation, that relates the cohesive shear traction at any point within the cohesive zone to the local rate of sliding was chosen to be of the form (see Fig. 4(b))

$$\tau(\dot{\delta}) = \tau_0 \left[1 + \beta C \frac{\dot{\delta}(\eta_1/L)}{c_s} \right], \quad -1 < \frac{\eta_1}{L} < 0, \tag{30}$$

where τ_0 is the cohesive shear strength of the material under quasi-static sliding, β is a dimensionless rate parameter, $\dot{\delta}(\eta_1/L) = \dot{u}_1(\eta_1/L, \eta_2 \to 0^+) - \dot{u}_1(\eta_1/L, \eta_2 \to 0^-)$ is the local sliding rate and C is another dimensionless parameter, chosen to be $\mu/(2\tau_0)$, so that at slip rates $\dot{\delta}$ of the order 10^1 m/s, β has the order of unity. Thus the cohesive shear traction at any point within the cohesive zone is given by

$$\tau\left(\frac{\eta_1}{L}\right) = \tau_0 \left[1 + \beta \frac{\mu}{2\tau_0} \frac{\dot{\delta}(\eta_1/L)}{c_s} \right], \quad -1 < \frac{\eta_1}{L} < 0. \tag{31}$$

Noting that $\dot{\delta}(\eta_1/L) = -2v u_{1,1}(\eta_1/L, \eta_2 \to 0^+)$ and substituting for $u_{1,1}$ from (17) and (29), we obtain

$$f(\eta_1) - \left\{ \beta \frac{v^3}{c_s^3} \frac{\alpha_s}{R(v)} \right\} \frac{1}{\pi} \mathrm{pv} \int_{-L}^{0} \frac{f(\xi)}{(\xi + |\eta_1|)} \, \mathrm{d}\xi = \frac{1}{\sqrt{|\eta_1|}}, \quad 0 \leqslant v < c_s, \tag{32a}$$

$$\hat{f}(\eta_1) \left\{ 1 + \beta \frac{v^3}{c_s^3} \frac{\hat{\alpha}_s}{R_q} \cos q\pi \right\} - \left\{ \beta \frac{v^3}{c_s^3} \frac{\hat{\alpha}_s}{R_q} \sin q\pi \right\} \frac{1}{\pi} \mathrm{pv} \int_{-L}^{0} \frac{\hat{f}(\xi)}{(\xi + |\eta_1|)} \, \mathrm{d}\xi$$

$$= \frac{1}{|\eta_1|^{1-q}}, \quad c_s < v < c_l, \tag{32b}$$

where

$$f(\eta_1) = \frac{\tau(\eta_1/L)}{\tau_0 \sqrt{|\eta_1|}}, \quad 0 \leqslant v < c_s, \tag{33}$$

$$\hat{f}(\eta_1) = \frac{\tau(\eta_1/L)}{\tau_0|\eta_1|^{1-q}}, \quad c_s < v < c_l. \tag{34}$$

Eq. (32) is a pair of singular integral equations of the Cauchy type, the solutions to which subject to the boundary conditions

$$\tau\left(\frac{\eta_1}{L} \to 0^-\right) \to \tau_0, \quad \sqrt{1+\frac{\eta_1}{L}}\,\tau(\eta_1/L \to -1^+) \to 0, \quad 0 \leqslant v < c_s, \tag{35a}$$

$$\tau\left(\frac{\eta_1}{L} \to 0^-\right) \to \tau_0 \quad \left(1+\frac{\eta_1}{L}\right)^q \tau(\eta_1/L \to -1^+) \to 0, \quad c_s < v < c_l \tag{35b}$$

give the unknown cohesive traction distributions, $\tau(-1 < \eta_1/L < 0)$ for the subsonic and intersonic cases, respectively. The boundary conditions (35) ensure that the singularity exponent at the physical crack tip is smaller than that in the case of a no cohesive zone. The solution procedure follows the methods given in Muskhelishvili (1963), Gakhov (1990), and is omitted.

5. Solution

The cohesive shear traction distribution is given by

$$\frac{\tau}{\tau_0}(-1 < \eta_1/L \leqslant 0) = \begin{cases} 1+\dfrac{\sin\gamma\pi}{\pi}\dfrac{(-\eta_1/L)^{\gamma+1/2}}{(1+\eta_1/L)^{\gamma}}\displaystyle\int_0^1 \frac{(1-s)^{\gamma}}{\sqrt{s}(1+s\eta_1/L)}\,\mathrm{d}s, & 0 \leqslant v < c_R, \\ 1+\dfrac{\sin\lambda\pi}{\pi}\dfrac{(-\eta_1/L)^{1-q+\lambda}}{(1+\eta_1/L)^{\lambda}}\displaystyle\int_0^1 \frac{(1-s)^{\lambda}}{s^q(1+s\eta_1/L)}\,\mathrm{d}s, & c_s < v < c_l, \end{cases} \tag{36}$$

where

$$\gamma = \frac{1}{\pi}\tan^{-1}\left\{\beta\frac{v^3}{c_s^3}\frac{\alpha_s}{R(v)}\right\}, \quad 0 \leqslant v < c_R, \tag{37}$$

$$\lambda = \frac{1}{\pi}\tan^{-1}\left\{\frac{\beta\dfrac{v^3}{c_s^3}\dfrac{\hat{\alpha}_s}{R_q}\sin q\pi}{1+\beta\dfrac{v^3}{c_s^3}\dfrac{\hat{\alpha}_s}{R_q}\cos q\pi}\right\}, \quad c_s < v < c_l \tag{38}$$

and the integrals in (36) converge for $-1 \leqslant \eta_1/L \leqslant 0$. As mentioned before, the crack speed regime $c_R < v < c_s$ is inadmissible for running mode II cracks from energetic considerations and henceforth we restrict ourselves to subRayleigh ($0 \leqslant v < c_R$) and intersonic regimes only. Unless mentioned, all the plots in this section and the next one are plotted for 2D plane stress and for $\nu = 0.34$ (Poisson's ratio of Homalite). From (36) one can see that γ and λ are the singularity exponents associated with shear stress at the physical crack tip ($\eta_1 = -L$). σ_{12} is singular at the crack tip, except in the trivial case of $\beta = 0$ (rate-independent Dugdale-type cohesive zone for which both γ and λ are identically zero). For a sharp crack (no cohesive zone), the singularity exponent at

subRayleigh speeds is $\frac{1}{2}$. With a rate-dependent cohesive zone, the singularity exponent γ is always less than $\frac{1}{2}$ and moreover it is a function of crack speed. As $v \to c_R$, $\gamma \to \frac{1}{2}$, i.e., as $v \to c_R$, the usual square root singular solution is recovered for any positive value of the rate parameter β. For a sharp crack with no cohesive zone, the singularity exponent at intersonic crack speeds is given by q, with its peak value of $\frac{1}{2}$ attained at $v = \sqrt{2}c_s$. With a rate-dependent cohesive zone, the singularity exponent λ is always less than q, is a function of crack speed and its peak value is attained at a speed higher than $\sqrt{2}c_s$. As the influence of rate sensitivity becomes greater with other factors held fixed, the strength of the crack edge singularity increases and the fraction of the yield zone over which the singular solution dominates becomes greater.

With the known cohesive shear traction (36) one can compute F'', G'' and g'' and thus obtain the dominant near-tip stress field. The stress field is given in Appendix A for both subRayleigh and intersonic crack speeds. The shear stress component σ_{12} on the crack plane ($\eta_2 \to 0^+$) is plotted in Fig. 5(a) for different intersonic crack speeds at a fixed $\beta = 0$ (rate-independent cohesive zone). For $\beta = 0$ and $\eta_2/L \to 0$:

$$\frac{\sigma_{12}}{\tau_0}(\eta_1/L > 0) = \begin{cases} \dfrac{2}{\pi}\left(\dfrac{\eta_1}{L}\right)^{-1/2}\left[1 - \dfrac{1}{2}\displaystyle\int_0^1 \frac{\sqrt{\xi}}{\xi + \eta_1/L}\,\mathrm{d}\xi\right], & 0 \leqslant v < c_R, \\ \dfrac{\sin q\pi}{q\pi}\left(\dfrac{\eta_1}{L}\right)^{-q}\left[1 - q\displaystyle\int_0^1 \frac{\xi^q}{\xi + \eta_1/L}\,\mathrm{d}\xi\right], & c_s < v < c_l, \end{cases} \tag{39}$$

where $\sigma_{12} = \tau_0$ within the cohesive zone and it vanishes on the crack faces. As seen, σ_{12} is bounded everywhere on the crack plane. Its variation is independent of crack speed in the subRayleigh regime, where as in the intersonic regime it is dependent on crack speed. The influence of the rate parameter β on the crack plane distribution of σ_{12} is shown in Fig. 5(b). The distribution is shown for different various values of β at a fixed intersonic speed $v = 1.47c_s$. For an intersonic mode II crack with a rate-dependent cohesive zone, σ_{12} on the crack plane ($\eta_2 \to 0^+$) is given by

$$\frac{\sigma_{12}}{\tau_0}(\eta_1/L > 0) = \frac{\sin q\pi}{\pi}\left(\frac{\eta_1}{L}\right)^{1-q}\left\{\int_0^1 \frac{\mathrm{d}\xi}{\xi^{1-q}(\xi + \eta_1/L)} + \int_0^1 \frac{\mathrm{d}s}{s^q(1 + s\eta_1/L)} - \left(\frac{\eta_1/L}{1 + \eta_1/L}\right)^{\lambda}\int_0^1 \frac{(1-s)^{\lambda}}{s^q(1 + s\eta_1/L)}\,\mathrm{d}s\right\}, \tag{40}$$

where σ_{12} within the cohesive zone is given in (36) and it vanishes on the crack faces. From Fig. 5(b) we can see that σ_{12} is singular at the physical crack tip, the strength of the singularity λ increasing with β. As $\beta \to \infty$, the distribution becomes the same as in the case of a singular solution with no cohesive zone.

The cohesive zone length L is determined by imposing a physical requirement that the stress intensity at the front end of the cohesive zone should vanish. Incorporating the known traction distribution from (36) into (16) and (28) one can obtain the length of the cohesive zone in terms of the far-field applied loading (σ_{12}^D), shear strength of the crack plane (τ_0), crack speed (v) and the rate parameter (β). Since the definition of stress intensity factor varies from subRayleigh to intersonic speeds, we choose σ_{12}^D

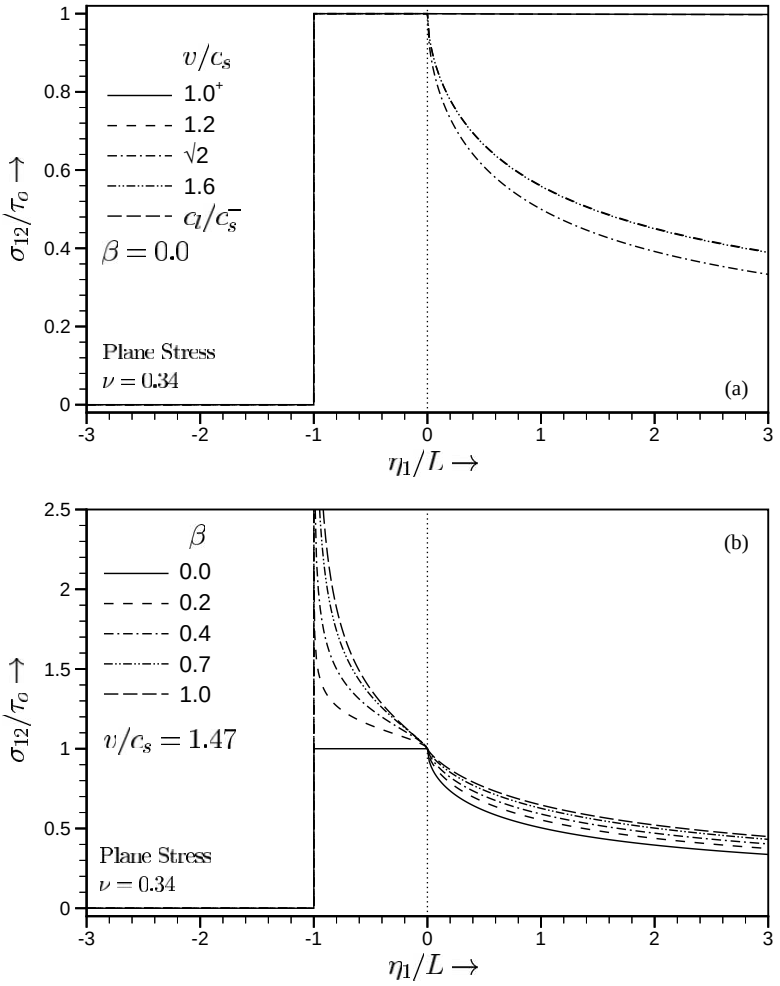

Fig. 5. Intersonically propagating mode II crack with a rate-dependent cohesive zone: (a) stress component σ_{12} on the crack plane for $\beta = 0.0$ and for different values of crack speed v; (b) stress component σ_{12} on the crack plane for $v/c_s = 1.47$ and for different values of rate parameter β.

as the measure of the amplitude of far-field applied loading. σ_{12}^D is the "remote" shear stress on the crack plane a distance $D \gg L$ ahead of the crack tip, where the usual singular solution for the case of a mathematically sharp crack with no cohesive zone is expected to apply.

$$\frac{L}{L_0} = \begin{cases} \dfrac{1}{\pi}\left[\dfrac{\Gamma(\gamma+1/2)}{\Gamma(\gamma+1)}\right]^2, & 0 \leqslant v < c_R, \\ \dfrac{4}{\pi^2}\left(\dfrac{q\pi}{\sin q\pi}\right)^{1/q}\left(\dfrac{\sigma_{12}^D}{\tau_0}\right)^{1/q-2}\left[\dfrac{\Gamma(\lambda-q+1)}{\Gamma(1-q)\Gamma(1+\lambda)}\right]^{1/q}, & c_s < v < c_l, \end{cases} \tag{41}$$

where $\Gamma(\cdot)$ is the standard Euler gamma function. The normalizing parameter L_0 is the length of the cohesive zone associated with a quasi-statically growing crack with the same far-field applied loading σ_{12}^D. It is given by

$$L_0 = \frac{\pi^2}{4}\left(\frac{\sigma_{12}^D}{\tau_0}\right)^2 D. \tag{42}$$

In effect, L/L_0 represents the dependence of the cohesive zone length on v, β and τ_0 under a constant σ_{12}^D.

Fig. 6(a) shows the sliding rate $\dot{\delta}_1(=\dot{\delta})$ on the crack plane for various intersonic speeds with a rate-independent cohesive zone ($\beta=0$) and Fig. 6(b) shows the influence of the rate parameter β on $\dot{\delta}_1$ at a particular value of the intersonic speed, $v = 1.47c_s$.

$$\frac{\dot{\delta}_1}{c_s}\left(-1 < \frac{\eta_1}{L} \leqslant 0\right) = \begin{cases} \dfrac{2}{\beta}\dfrac{\tau_0}{\mu}\dfrac{\sin\gamma\pi}{\pi}\dfrac{(-\eta_1/L)^{\gamma+1/2}}{(1+\eta_1/L)^{\gamma}}\displaystyle\int_0^1 \frac{(1-s)^{\gamma}}{\sqrt{s}(1+s\eta_1/L)}\,\mathrm{d}s, & 0 \leqslant v < c_R, \\ \dfrac{2}{\beta}\dfrac{\tau_0}{\mu}\dfrac{\sin\lambda\pi}{\pi}\dfrac{(-\eta_1/L)^{1-q+\lambda}}{(1+\eta_1/L)^{\lambda}}\displaystyle\int_0^1 \frac{(1-s)^{\lambda}}{s^q(1+s\eta_1/L)}\,\mathrm{d}s, & c_s < v < c_l, \end{cases} \tag{43}$$

where $\dot{\delta}_1$ is singular at the crack tip, however through most of the cohesive zone, $\dot{\delta}_1$ is about $\approx 2\%$ of c_s for subRayleigh speeds and is about $\approx 4\%$ of c_s for intersonic speeds. 2–4% of c_s corresponds to sliding rates of a few m/s, consistent with our expectation while choosing the cohesive law. Also the rate parameter does not seem to have much of an influence on the variation of $\dot{\delta}_1$ within the cohesive zone, though the effect is a bit more pronounced for intersonic speeds.

The dynamic energy release rate G, defined as the energy flux into the crack tip region per unit crack advance per unit thickness may be expressed as (see Freund, 1990)

$$G = 2\int_0^{-L} \sigma_{12}(\eta_1, \eta_2 \to 0^+) u_{1,1}(\eta_1, \eta_2 \to 0^+)\,\mathrm{d}\eta_1. \tag{44}$$

With a rate-independent cohesive zone ($\beta = 0$), the dynamic energy release rate G is given by

$$\frac{G}{G_0} = \begin{cases} \dfrac{2\alpha_s(\alpha_1^2 - \alpha_s^2)}{R(v)}, & 0 \leqslant v < c_R, \\ \dfrac{4}{\pi^2}\dfrac{\hat{\alpha}_s(\alpha_1^2 + \hat{\alpha}_s^2)}{R_q}\dfrac{\sin q\pi}{1-q}\left(\dfrac{q\pi}{\sin q\pi}\right)^{1/q}\left(\dfrac{\sigma_{12}^D}{\tau_0}\right)^{1/q-2}, & c_s < v < c_l, \end{cases} \tag{45}$$

where G_0 is the energy release rate associated with a quasi-statically propagating crack with the same far-field applied load σ_{12}^D. G_0 is given by

$$G_0 = \frac{\pi(\kappa+1)}{4}\frac{\sigma_{12}^{D^2} D}{\mu}. \tag{46}$$

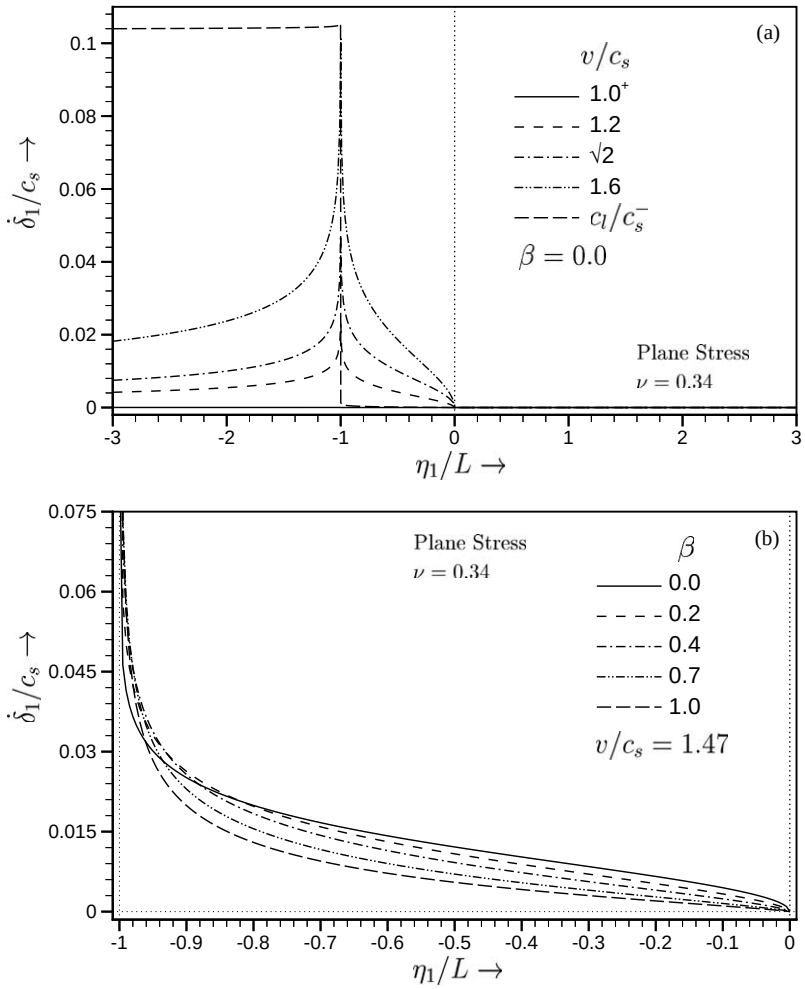

Fig. 6. Intersonically propagating mode II crack with a rate-dependent cohesive zone: (a) Relative sliding rate $\dot{\delta}_1$ on the crack plane for $\beta = 0.0$ and different values of the intersonic crack speed v; (b) relative sliding rate $\dot{\delta}_1$ on the crack plane for $v/c_s = 1.47$ and different values of the rate parameter β.

Fig. 7 shows the variation of the G/G_0 with crack speed for different values of σ_{12}^D/τ_0. For steady subRayleigh crack growth G is path independent and hence the process zone characteristics need not be taken into account as long as an annular region around the crack tip exists, where the square root singular fields are dominant. However, for intersonic speeds, G is dependent on the size and characteristics of the process zone. As seen from Fig. 7, the dynamic energy release rate G is finite through out the intersonic regime except for crack speeds close to c_s and c_l, where it vanishes. Hence, based on the requirement of a positive energy flux, the entire intersonic regime is admissible for

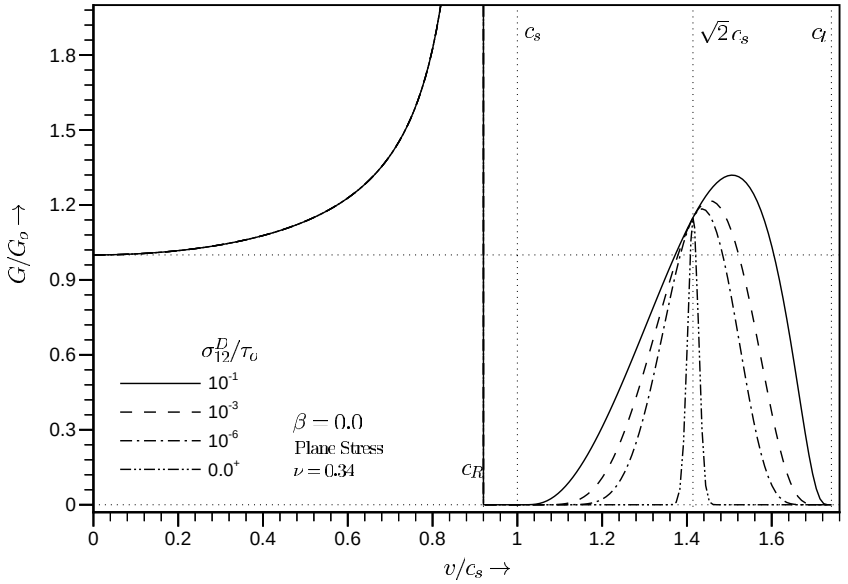

Fig. 7. Dynamically propagating mode II crack with a Dugdale-type cohesive zone—dependence of the normalized energy release rate G/G_0 on crack speed v, plotted for different values of σ_{12}^D/τ_0.

mode II crack growth. The variation of G/G_0 for intersonic speeds depends strongly on the shear strength of the fracture plane τ_0. As $\tau_0 \to \infty$, the singular solution with no cohesive zone is recovered and once again there exists only one intersonic speed $v = \sqrt{2}c_s$, at which the dynamic energy release rate is finite. With a lower shear strength more of the intersonic regime becomes admissible, the energy flux into the crack tip increases and also the energy flux attains its peak at a speed higher than $\sqrt{2}c_s$. At $v = \sqrt{2}c_s$, an intersonic crack behaves "subsonic like", i.e., the explicit dependence on τ_0 disappears and G attains a constant value equal to $2/\sqrt{(1+\kappa)(3-\kappa)}G_0$.

For a rate-dependent cohesive zone ($\beta > 0$):

$$\frac{G}{G_0} = \begin{cases} \dfrac{1}{\beta}\dfrac{(\alpha_l^2 - \alpha_s^2)}{v^3/c_s^3}\left[\dfrac{\Gamma(\gamma+1/2)}{\Gamma(1+\gamma)}\right]^2 g(\gamma), & 0 \leqslant v < c_R, \\ \dfrac{4}{\pi}\dfrac{1}{\beta}\dfrac{(\alpha_l^2 + \hat{\alpha}_s^2)}{v^3/c_s^3}\left(\dfrac{q\pi}{\sin q\pi}\right)^{1/q}\left(\dfrac{\sigma_{12}^D}{\tau_0}\right)^{1/q-2} & \\ \quad \times \left[\dfrac{\Gamma(\lambda - q + 1)}{\Gamma(1-q)\Gamma(1+\lambda)}\right]^{1/q} g^*(\lambda, q), & c_s < v < c_l, \end{cases} \tag{47}$$

where

$$g(\gamma) = 2\gamma + \frac{\sin^2\gamma\pi}{\pi^2}\int_0^1 \frac{\xi^{2\gamma+1}}{(1-\xi)^{2\gamma}}\left[\int_0^1 \frac{(1-s)^\gamma}{\sqrt{s}(1-s\xi)}\,\mathrm{d}s\right]^2 \mathrm{d}\xi, \quad 0 \leqslant v < c_R, \tag{48a}$$

$$g^*(\lambda,q)=\frac{\lambda}{1-q}+\frac{\sin^2\lambda\pi}{\pi^2}\int_0^1\frac{\xi^{2-2q+2\lambda}}{(1-\xi)^{2\lambda}}\left[\int_0^1\frac{(1-s)^\lambda}{s^q(1-s\xi)}\,\mathrm{d}s\right]^2\mathrm{d}\xi,\quad c_\mathrm{s}<v<c_\mathrm{l}. \tag{48b}$$

For subRayleigh crack speeds, G is path independent and hence there is no effect of β, whereas for intersonic speeds, the influence of β is small.

6. Critical crack tip sliding displacement criterion

Now we implement the second part of our cohesive law, i.e., we introduce a propagation criterion, which states that sustained dynamic mode II crack growth at any subRayleigh or intersonic speed, occurs under a constant crack tip sliding displacement (see Fig. 4(b)).

$$\delta_\mathrm{t}=u_1(\eta_1=-L,\eta_2\to 0^+)-u_1(\eta_1=-L,\eta_2\to 0^-)=\delta_\mathrm{t}^\mathrm{c}, \tag{49}$$

where $\delta_\mathrm{t}^\mathrm{c}$ is the critical crack tip sliding displacement, a material-specific parameter. Such a propagation criterion, which is concerned only with the local state in the vicinity of the crack tip is more convenient (as compared to a non-local criterion like the Griffith's criterion) for modeling the actual physical mechanism of crack growth as well as for application to practical problems using numerical techniques. Also, unlike in the subsonic case, for an intersonic crack, the process zone characteristics need to be known to determine the energy flux to the tip region and hence the advantage of employing a small-scale yielding type approach is lost. The crack tip sliding displacement, δ_t can be obtained by integrating (43) along the cohesive surface

$$\frac{\delta_\mathrm{t}}{\delta_\mathrm{t}^0}=\begin{cases}\dfrac{2\gamma}{\beta}\dfrac{(\alpha_\mathrm{l}^2-\alpha_\mathrm{s}^2)}{(v^3/c_\mathrm{s}^3)}\left[\dfrac{\Gamma(\gamma+1/2)}{\Gamma(\gamma+1)}\right]^2, & 0\leqslant v<c_\mathrm{R},\\[2ex] \dfrac{4\lambda}{\pi\beta(1-q)}\dfrac{(\alpha_\mathrm{l}^2+\hat{\alpha}_\mathrm{s}^2)}{(v^3/c_\mathrm{s}^3)}\left(\dfrac{q\pi}{\sin q\pi}\right)^{1/q} & \\ \quad\times\left(\dfrac{\sigma_{12}^D}{\tau_0}\right)^{1/q-2}\left[\dfrac{\Gamma(\lambda-q+1)}{\Gamma(1-q)\Gamma(1+\lambda)}\right]^{1/q}, & c_\mathrm{s}<v<c_\mathrm{l},\end{cases} \tag{50}$$

where δ_t^0 is the crack tip sliding displacement associated with a quasi-statically growing mode II crack under a far-field loading σ_{12}^D and a shear strength τ_0:

$$\delta_\mathrm{t}^0=\frac{\pi(\kappa+1)}{4}\frac{\tau_0}{\mu}\left(\frac{\sigma_{12}^D}{\tau_0}\right)^2 D. \tag{51}$$

The critical crack tip sliding displacement criterion (49) states that $\delta_\mathrm{t}=\delta_\mathrm{t}^0=\delta_\mathrm{t}^\mathrm{c}$. Hence (50) gives a relationship between the critical values (required to satisfy the criterion) of σ_{12}^D, v, β and τ_0.

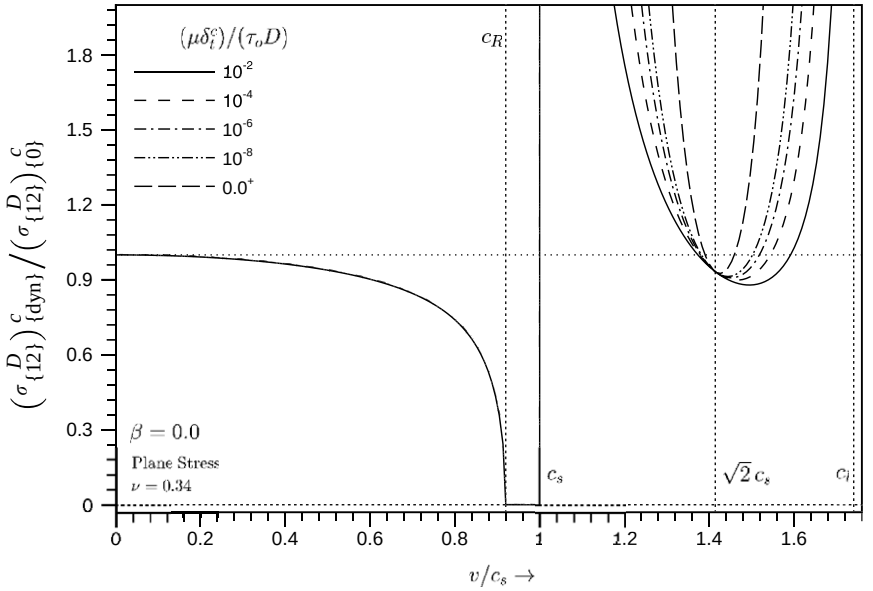

Fig. 8. Dynamically propagating mode II crack with a Dugdale-type cohesive zone—stability of crack growth. Dependence of the critical far-field load (required to sustain dynamic crack growth) on crack tip speed v, plotted for different values of the interface strength parameter $(\mu\delta_t^c)/(\tau_0 D)$.

Fig. 8 shows the variation of the critical far-field load $(\sigma_{12}^D)_{\rm dyn}^{\rm c}$ (required to satisfy the critical crack tip sliding displacement criterion (49)) with crack speed, for different values of τ_0 and at $\beta = 0$. The ratio $(\sigma_{12}^D)_{\rm dyn}^{\rm c}/(\sigma_{12}^D)_0^{\rm c}$ is given by (for $\beta = 0$)

$$\frac{(\sigma_{12}^D)_{\rm dyn}^{\rm c}}{(\sigma_{12}^D)_0^{\rm c}} = \begin{cases} \sqrt{\left[\dfrac{R(v)}{2\alpha_{\rm s}(\alpha_{\rm l}^2-\alpha_{\rm s}^2)}\right]}, & 0 \leqslant v < c_{\rm R}, \\ \left(\dfrac{\mu\delta_{\rm t}^{\rm c}}{D\tau_0}\right)^{q-1/2} \sqrt{\left[\dfrac{\pi}{2}\dfrac{(1+\hat{\alpha}_{\rm s}^2)}{(\alpha_{\rm l}^2+\hat{\alpha}_{\rm s}^2)}\right]} & \\ \quad \times \left(\dfrac{\sin q\pi}{q\pi}\right)\left[\dfrac{2\pi\alpha_{\rm l}(1-q)}{(1+\hat{\alpha}_{\rm s}^2)\sin^2 q\pi}\right]^q, & c_{\rm s} < v < c_{\rm l}, \end{cases} \tag{52}$$

where the critical far-field load required for quasi-static crack propagation, $(\sigma_{12}^D)_0^{\rm c}$ is given by

$$(\sigma_{12}^D)_0^{\rm c} = \tau_0\sqrt{\frac{4}{(\kappa+1)\pi}\frac{\mu\delta_{\rm t}^{\rm c}}{D\tau_0}}. \tag{53}$$

As seen from Fig. 8, for a subRayleigh crack, the far-field load required to sustain a small acceleration in crack speed is lower compared to its previous value. This situation may be interpreted as an instability and it can be expected that a subsonic mode II crack would accelerate rapidly to $c_{\rm R}$. This explains the reason for non-observation of

any subsonic crack speeds for mode II shear cracks propagating along a weak plane in Homalite (see Fig. 3(b)). Even if the shear crack initiating from the notch initially propagated at subRayleigh speeds, it would immediately accelerate to c_R and beyond. By the same interpretation, for an intersonic crack, there is an initially unstable speed regime followed by a stable speed regime. The critical far-field load $(\sigma_{12}^D)_{dyn}^c/(\sigma_{12}^D)_0^c$ is also a function of a material parameter $(\mu\delta_t^c)/(\tau_0 D)$ in the intersonic regime. μ and δ_t^c are material constants and D is an arbitrary distance ahead of the crack tip at which the singular solution with no cohesive zone dominates. Hence the parameter $(\mu\delta_t^c)/(\tau_0 D)$ may be interpreted as a measure of shear strength of the fracture plane. It is seen that the entire speed regime $c_s < v < \sqrt{2}c_s$ is unstable and the speed at which intersonic crack propagation becomes stable depends on the shear strength of the fracture plane. For $\tau_0 \to 0$, i.e., for the case of vanishing shear strength of the fracture plane, almost the entire intersonic regime becomes unstable, indicating that a mode II crack on a weak plane of vanishing strength should propagate at speeds close to c_l. On the other hand, for $\tau_0 \to \infty$, the singular solution with no cohesive zone is recovered and the onset of stability occurs at $v = \sqrt{2}c_s$. Similar observations that the speed regime $\sqrt{2}c_s < v < c_l$ is stable for intersonic mode II crack growth were made by Burridge et al. (1979), Freund (1979). For more realistic values of the parameter $(\mu\delta_t^c)/(\tau_0 D) \approx 10^{-2}$–$10^{-3}$, the critical load required to sustain intersonic crack propagation is a minimum between $\sqrt{2}c_s$ and 1.5. This explains the observed experimental behavior of crack speed, where the intersonic mode II crack was found to accelerate to speeds close to c_l and then as the loading pulse was cut-off, settled down to a stable propagation speed close to $\sqrt{2}c_s$. Such a crack speed behavior was also observed by Needleman 1999 in his numerical simulations of mode II crack growth along a weak plane. A portion of rupture front during the 1999 Turkey Earthquake was also found to propagate at $\sqrt{2}c_s$ (Bouchon et al., 2001).

Fig. 9 shows the effect of the rate parameter β on the critical far-field load for both subRayleigh and intersonic mode II crack propagation, with a chosen value of the material parameter $(\mu\delta_t^c)/(\tau_0 D) = 0.01$.

$$\frac{(\sigma_{12}^D)_{dyn}^c}{(\sigma_{12}^D)_0^c} = \begin{cases} \sqrt{\left[\frac{1}{2}\frac{\beta}{\gamma}\frac{v^3/c_s^3}{\alpha_l^2-\alpha_s^2}\right]}\,\frac{\Gamma(\gamma+1)}{\Gamma(\gamma+1/2)}, & 0 \leqslant v < c_R, \\ \left(\frac{\mu\delta_t^c}{D\tau_0}\right)^{q-1/2}\left[\frac{\beta}{2\lambda}\frac{v}{c_s}(1-q)\right]^q \sqrt{\left[\frac{\pi}{2}\frac{1+\hat{\alpha}_s^2}{\alpha_l^2+\hat{\alpha}_s^2}\right]} & \\ \quad \times\left(\frac{\sin q\pi}{q\pi}\right)\frac{\Gamma(1-q)\Gamma(1+\lambda)}{\Gamma(\lambda-q+1)}, & c_s < v < c_l. \end{cases} \tag{54}$$

Unlike for a rate-independent cohesive zone, subRayleigh mode II crack growth with a rate-dependent cohesive zone is stable up to a threshold speed, beyond which it would accelerate unstably to c_R. As $v \to c_R$, $(\sigma_{12}^D)_{dyn}^c/(\sigma_{12}^D)_0^c$ attains a finite value equal to $\sqrt{\beta c_R \pi/(2c_s(1+\nu))}$. For intersonic mode II crack growth with a rate-dependent cohesive zone, it is seen that increasing rate sensitivity increases the level of the critical load required as well as moves the crack speed corresponding to the onset

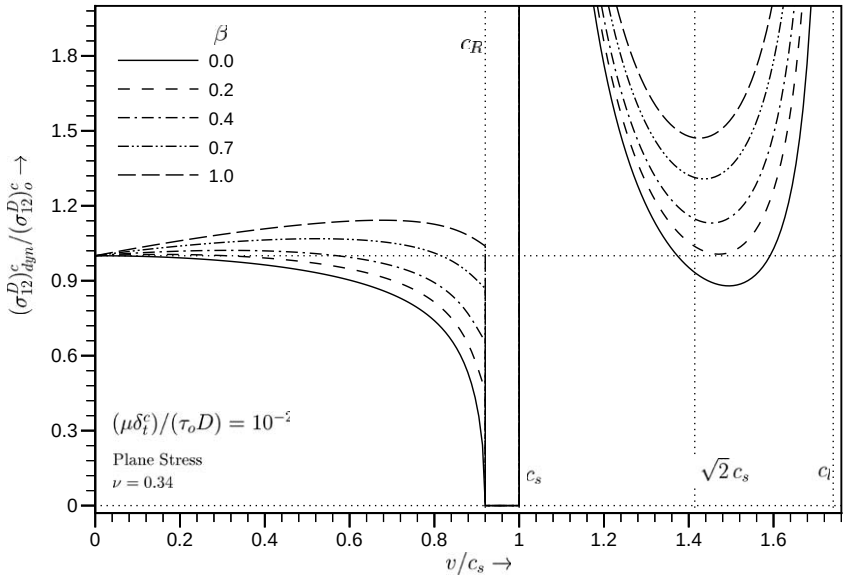

Fig. 9. Dynamically propagating mode II crack with a rate-dependent cohesive zone—stability of crack growth. Dependence of the critical far-field load (required to sustain dynamic crack growth) on crack tip speed v, plotted for $(\mu\delta_t^c)/(\tau_0 D) = 10^{-2}$ and for different values of the rate parameter β.

of instability closer towards $\sqrt{2}c_s$. Here, it must be understood that stability results obtained for a steadily moving semi-infinite crack may be significantly different from those for cracks with more realistic geometries. Broberg (1994, 1995) showed that for a symmetrically expanding mode II crack under uniform remote shear loading, the entire intersonic regime is unstable and that such a crack would accelerate all the way up to c_l. Burridge et al. (1979) argued that instability is more pronounced in the case of finite cracks undergoing transient crack growth. If a particular speed regime is found to be unstable for a moving steady-state semi-infinite crack, then the possibility that it would also be unstable for an expanding finite crack is very high.

The normalized critical cohesive zone length, L^c_{dyn}/L^c_0 is given by

$$\frac{L^c_{dyn}}{L^c_0} = \begin{cases} \dfrac{1}{2\pi}\dfrac{\beta}{\gamma}\dfrac{v}{c_s}\dfrac{1-\alpha_s^2}{\alpha_l^2-\alpha_s^2}, & 0 \leqslant v < c_R, \\ \dfrac{1-q}{\pi}\dfrac{\beta}{\lambda}\dfrac{v}{c_s}\dfrac{1+\hat{\alpha}_s^2}{\alpha_l^2+\hat{\alpha}_s^2}, & c_s < v < c_l, \end{cases} \tag{55}$$

where, the critical cohesive zone length for quasi-static crack propagation

$$L^c_0 = \frac{\pi(\kappa+1)}{16}\left(\frac{\mu\delta_t^c}{\tau_0}\right). \tag{56}$$

The critical cohesive zone size for subRayleigh speeds, was found to decrease monotonically up to c_R. It vanishes at c_R in the case of a rate-independent cohesive zone,

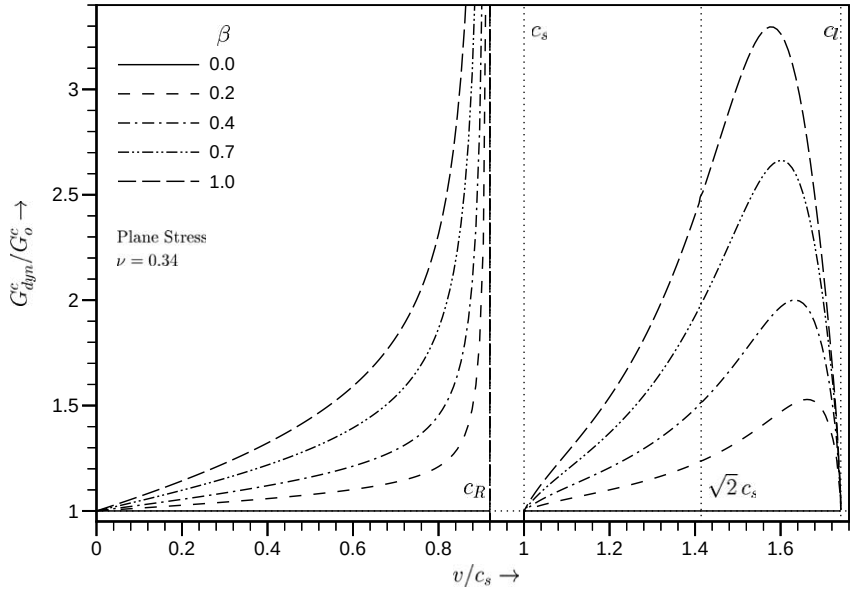

Fig. 10. Dynamically propagating mode II crack with a rate-dependent cohesive zone—variation of the critical dynamic energy release rate (fracture energy required to sustain dynamic crack growth) with crack tip speed v, plotted for different values of the rate parameter β.

whereas it attains a finite value equal to $2\beta c_{\mathrm{R}}/(\pi(1+\nu)c_{\mathrm{s}})$ at c_{R} for any +ve β. Andrews (1976) in a numerical simulation of a symmetrically expanding mode II crack under the action of remote uniform shear stresses found that the cohesive zone size decreases continuously with crack speed in the subRayleigh regime attaining its minimum value at c_{R}. Such a behavior was also observed in the numerical simulations of Geubelle and Kubair (2001). In the intersonic case, the cohesive zone size is always finite and positive. Such an observation was used by Yu and Suo (2000) to justify the admissibility of mode II intersonic crack growth. The critical cohesive zone length is found to be rather insensitive to the rate parameter β.

Fig. 10 shows the variation of critical dynamic energy release rate (rate-dependent fracture energy) with crack speed for different values of the rate parameter β.

$$\frac{G^{\mathrm{c}}_{\mathrm{dyn}}}{G^{\mathrm{c}}_0} = \begin{cases} \dfrac{1}{2\gamma} g(\gamma) = \dfrac{\beta}{\gamma}\dfrac{v^3}{c_{\mathrm{s}}^3}\dfrac{\alpha_{\mathrm{s}}}{R(v)}\left[\dfrac{\Gamma(\gamma+1)}{\Gamma(\gamma+1/2)}\right]^2, & 0 \leqslant v < c_{\mathrm{R}}, \\ \dfrac{1-q}{\lambda} g^*(\lambda, q), & c_{\mathrm{s}} < v < c_{\mathrm{l}}, \end{cases} \tag{57}$$

where the critical energy release rate for quasi-static crack propagation

$$G^{\mathrm{c}}_0 = \tau_0 \delta^{\mathrm{c}}_{\mathrm{t}}. \tag{58}$$

The material/specimen dependent "fracture energy vs crack speed" curve is strongly influenced by the rate parameter β. It is found that for a rate-dependent cohesive zone

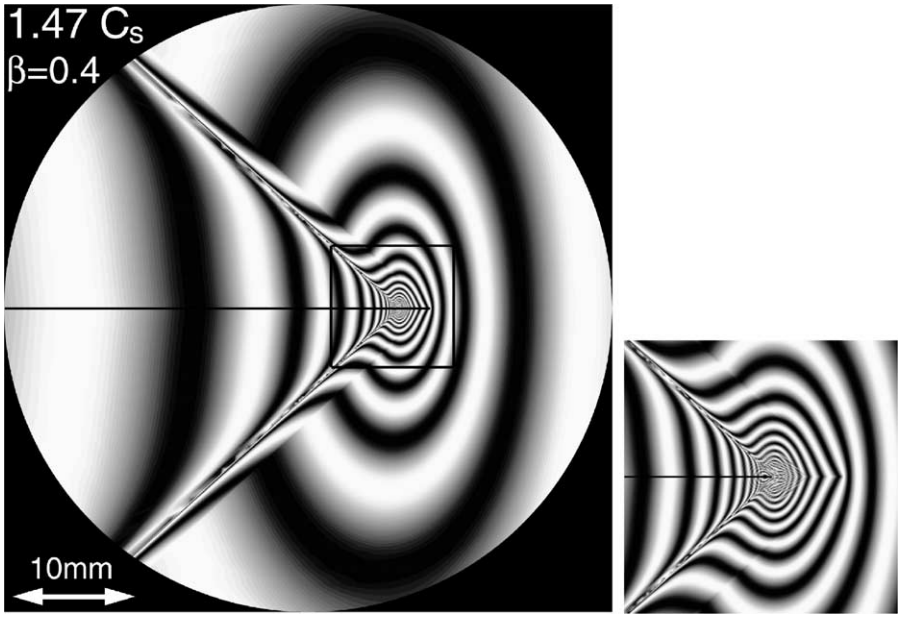

Fig. 11. Isochromatic fringe pattern around a propagating intersonic mode II crack with a rate-dependent cohesive zone. The propagating crack obeys a critical crack tip sliding displacement criterion with $\delta_t^c \approx 21$ μm and $\mu/\tau_0 = 136$. Also $v/c_s = 1.47$, $\beta = 0.4$ and $L_{dyn}^c = 2.5$ mm. A magnified view of the region around the crack tip (enclosed in the black rectangle) is shown on the right.

($\beta > 0$), the dissipated fracture energy (required to sustain mode II crack growth) into the tip region blows up as $v \to c_R$, suggesting that a subsonic mode II crack would encounter ever increasing resistance as it approaches c_R. In the intersonic regime, G_{dyn}^c/G_0^c is finite and positive throughout, with a peak in dissipated fracture energy at a speed higher than $\sqrt{2}c_s$. The fracture energy is found to depend strongly on the rate parameter β, with higher energy dissipated with increasing rate sensitivity. Thus the importance of the curious speed of $\sqrt{2}c_s$ (vis-a-vis energy flux into the tip) is diminished.

Fig. 11 shows the theoretically predicted isochromatic fringe pattern around an intersonically propagating mode II crack. The crack propagates with a line cohesive zone in front of the tip and also obeys the critical crack tip sliding displacement criterion. The intersonic crack was assumed to be propagating at $1.47c_s$ and the cohesive law was assumed to be rate dependent ($\beta = 0.4$). In both cases, the ratio of shear modulus to the shear strength of the weak plane (μ/τ_0) was chosen to be 136, approximating the case of Homalite/Homalite bonded specimen used in the experiments. The critical crack tip sliding displacement was chosen to be 21 μm. This ensures that the critical cohesive zone length determined from (55) and (56) would lie between 2 and 3 mm (for intersonic speeds close to $\sqrt{2}c_s$), which is approximately the width of the Mach wave seen in Fig. 3(a).

The field of view shown in Fig. 11 has a 50 mm diameter and the front end of the cohesive zone is located on the horizontal diameter about 35 mm from the left edge of the field of view. The cohesive zone length ($v = 1.47c_s$) was found to be 2.5 mm for $\beta = 0.4$. We see that the presence of a cohesive zone gives a finite width to the Mach waves emanating from the tip region. Comparing it with the experimental fringe pattern shown in Fig. 3(a), we see that the patterns are similar in a small region close to the crack tip. Also, the fringe pattern within the finite width of the Mach waves, seems to be qualitatively similar. The range of dominance of the current solution seems to be of the order of about 20 mm.

7. Summary

1. Experimental evidence is provided of intersonic mode II cracks along a weak plane joining two identical Homalite-100 plates.
2. The observed mode II crack speeds span the entire intersonic regime. Also the Mach waves radiating from the intersonic crack tip have a finite width. Such features could not be explained based on the Freund's singular solution for an intersonic mode II crack, thus motivating our study based on a cohesive zone model.
3. Subsonic and Intersonic mode II crack propagation with a rate-dependent cohesive zone is analyzed. A cohesive law is chosen, wherein the cohesive shear traction depends linearly on the local sliding rate. Complete decohesion is assumed to occur when the crack tip sliding displacement reaches a material-specific critical value. Explicit expressions are obtained for the near-tip stress and particle velocity fields.
4. With the rate-dependent cohesive zone model, it is found that the fracture energy is finite through out the intersonic regime. The importance of the curious speed $\sqrt{2}c_s$ is diminished, and the energy dissipated is found to be higher at intersonic speeds closer to c_l. Fracture energy was found to be a strong function of rate sensitivity, increasing with increasing value of the rate parameter.
5. Investigation of the behavior of required far-field loads, indicated that the subsonic regime is inherently unstable for mode II cracks. However, with increasing rate sensitivity, stable mode II crack growth was found to be possible at low subsonic speeds. Mode II crack growth at intersonic speeds was found to be unstable up to a critical speed higher than $\sqrt{2}c_s$, beyond which it was found to be stable, thus explaining the observed crack speed behavior in the experiments. With decreasing strength of the crack plane, it was found that an intersonic mode II crack would accelerate all the way up to c_l, whereas increasing strength of the crack plane seems to favor stable crack growth at speeds close to $\sqrt{2}c_s$.
6. Isochromatic fringe patterns were generated using the crack tip fields around an intersonic mode II crack with a rate-dependent cohesive zone. They agree reasonably well with the experimentally recorded patterns, especially close to the crack tip. The Mach waves were found to be of finite width, the isochromatic fringe pattern within which was also qualitatively similar to that observed in the experimental patterns.

Acknowledgements

The authors gratefully acknowledge the support of the National Science Foundation (Grant No. CMS9813100 and Grant No. CMS9983779) and of the Office of Naval Research (Grant No. N00014-95-1-0453, Dr. Y.D.S. Rajapakse, Project Monitor). Many helpful discussions with Prof. J.R. Rice of Harvard University and Prof. A. Needleman of Brown University are also acknowledged.

Appendix A. Near-tip stress fields

For a subsonic mode II crack with a rate-independent cohesive zone ($\beta = 0$):

$$\frac{\sigma_{11}}{\tau_0} = \frac{4\alpha_s}{\pi R(v)}\left[\frac{(1+2\alpha_l^2-\alpha_s^2)}{\sqrt{r_l/L}}\left\{-\sin\left(\frac{\theta_l}{2}\right) + \frac{1}{2}\int_0^1 \frac{\sqrt{\zeta}[\zeta\sin(\theta_l/2)+(r_l/L)\sin(3\theta_l/2)]}{\zeta^2+(r_l/L)^2+2\zeta(r_l/L)\cos\theta_l}\,d\zeta\right\} - \frac{(1+\alpha_s^2)}{\sqrt{r_s/L}} \times \left\{-\sin\left(\frac{\theta_s}{2}\right) + \frac{1}{2}\int_0^1 \frac{\sqrt{\zeta}[\zeta\sin(\theta_s/2)+(r_s/L)\sin(3\theta_s/2)]}{\zeta^2+(r_s/L)^2+2\zeta(r_s/L)\cos\theta_s}\,d\zeta\right\}\right], \quad \text{(A.1a)}$$

$$\frac{\sigma_{22}}{\tau_0} = \frac{4\alpha_s(1+\alpha_{s)}^2}{\pi R(v)}\left[\frac{-1}{\sqrt{r_l/L}}\left\{-\sin\left(\frac{\theta_l}{2}\right) + \frac{1}{2}\int_0^1 \frac{\sqrt{\zeta}[\zeta\sin(\theta_l/2)+(r_l/L)\sin(3\theta_l/2)]}{\zeta^2+(r_l/L)^2+2\zeta(r_l/L)\cos\theta_l}\,d\zeta\right\} - \frac{(1+\alpha_s^2)}{\sqrt{r_s/L}} \times \left\{-\sin\left(\frac{\theta_s}{2}\right) + \frac{1}{2}\int_0^1 \frac{\sqrt{\zeta}[\zeta\sin(\theta_s/2)+(r_s/L)\sin(3\theta_s/2)]}{\zeta^2+(r_s/L)^2+2\zeta(r_s/L)\cos\theta_s}\,d\zeta\right\}\right], \quad \text{(A.1b)}$$

$$\frac{\sigma_{12}}{\tau_0} = \frac{2}{\pi R(v)}\left[\frac{-4\alpha_l\alpha_s}{\sqrt{r_l/L}}\left\{-\cos\left(\frac{\theta_l}{2}\right) + \frac{1}{2}\int_0^1 \frac{\sqrt{\zeta}[\zeta\cos(\theta_l/2)+(r_l/L)\cos(3\theta_l/2)]}{\zeta^2+(r_l/L)^2+2\zeta(r_l/L)\cos\theta_l}\,d\zeta\right\} - \frac{(1+\alpha_s^2)^2}{\sqrt{r_s/L}}\left\{-\cos\left(\frac{\theta_s}{2}\right) + \frac{1}{2}\int_0^1 \frac{\sqrt{\zeta}[\zeta\cos(\theta_s/2)+(r_s/L)\cos(3\theta_s/2)]}{\zeta^2+(r_s/L)^2+2\zeta(r_s/L)\cos\theta_s}\,d\zeta\right\}\right], \quad \text{(A.1c)}$$

where

$$r_s = \sqrt{\eta_1^2 + \alpha_s^2 \eta_2^2}, \quad \theta_s = \tan^{-1}\left[\frac{\alpha_s \eta_2}{\eta_1}\right], \tag{A.2a}$$

$$r_l = \sqrt{\eta_1^2 + \alpha_l^2 \eta_2^2}, \quad \theta_l = \tan^{-1}\left[\frac{\alpha_l \eta_2}{\eta_1}\right]. \tag{A.2b}$$

For a subsonic mode II crack with a rate-dependent cohesive zone ($\beta > 0$):

$$\begin{aligned}\frac{\sigma_{11}}{\tau_0} = \frac{2\alpha_s}{\pi R(v)} \Bigg[& (1 + 2\alpha_l^2 - \alpha_s^2)\sqrt{\frac{r_l}{L}} \sin\left(\frac{\theta_l}{2}\right) \\ & \times \left\{ \int_0^1 \frac{[\zeta - (r_l/L)]}{\sqrt{\zeta}[\zeta^2 + (r_l/L)^2 + 2\zeta(r_l/L)\cos\theta_l]}\, \mathrm{d}\zeta + \frac{\sin\gamma\pi}{\pi} \int_0^1 \left(\frac{\zeta}{1-\zeta}\right)^{\gamma} \right. \\ & \left. \times \frac{[\zeta - (r_l/L)]}{[\zeta^2 + (r_l/L)^2 + 2\zeta(r_l/L)\cos\theta_l]} \int_0^1 \frac{(1-s)^{\gamma}}{\sqrt{s}(1 - s\zeta)}\, \mathrm{d}s\, \mathrm{d}\zeta \right\} \\ & - (1 + \alpha_s^2)\sqrt{\frac{r_s}{L}} \sin\left(\frac{\theta_s}{2}\right) \left\{ \int_0^1 \frac{[\zeta - (r_s/L)]}{\sqrt{\zeta}[\zeta^2 + (r_s/L)^2 + 2\zeta(r_s/L)\cos\theta_s]}\, \mathrm{d}\zeta \right. \\ & + \frac{\sin\gamma\pi}{\pi} \int_0^1 \left(\frac{\zeta}{1-\zeta}\right)^{\gamma} \frac{[\zeta - (r_s/L)]}{[\zeta^2 + (r_s/L)^2 + 2\zeta(r_s/L)\cos\theta_s]} \\ & \left. \times \int_0^1 \frac{(1-s)^{\gamma}}{\sqrt{s}(1 - s\zeta)}\, \mathrm{d}s\, \mathrm{d}\zeta \right\} \Bigg], \end{aligned} \tag{A.3a}$$

$$\begin{aligned}\frac{\sigma_{22}}{\tau_0} = \frac{2\alpha_s}{\pi R(v)} \Bigg[& -(1 + \alpha_s^2)\sqrt{\frac{r_l}{L}} \sin\left(\frac{\theta_l}{2}\right) \\ & \times \left\{ \int_0^1 \frac{[\zeta - (r_l/L)]}{\sqrt{\zeta}[\zeta^2 + (r_l/L)^2 + 2\zeta(r_l/L)\cos\theta_l]}\, \mathrm{d}\zeta + \frac{\sin\gamma\pi}{\pi} \int_0^1 \left(\frac{\zeta}{1-\zeta}\right)^{\gamma} \right. \\ & \left. \times \frac{[\zeta - (r_l/L)]}{[\zeta^2 + (r_l/L)^2 + 2\zeta(r_l/L)\cos\theta_l]} \int_0^1 \frac{(1-s)^{\gamma}}{\sqrt{s}(1 - s\zeta)}\, \mathrm{d}s\, \mathrm{d}\zeta \right\} \\ & + (1 + \alpha_s^2)\sqrt{\frac{r_s}{L}} \sin\left(\frac{\theta_s}{2}\right) \left\{ \int_0^1 \frac{[\zeta - (r_s/L)]}{\sqrt{\zeta}[\zeta^2 + (r_s/L)^2 + 2\zeta(r_s/L)\cos\theta_s]}\, \mathrm{d}\zeta \right. \end{aligned}$$

$$+\frac{\sin\gamma\pi}{\pi}\int_0^1\left(\frac{\zeta}{1-\zeta}\right)^{\gamma}\frac{[\zeta-(r_s/L)]}{[\zeta^2+(r_s/L)^2+2\zeta(r_s/L)\cos\theta_s]}$$
$$\times\int_0^1\frac{(1-s)^{\gamma}}{\sqrt{s}(1-s\zeta)}\,\mathrm{d}s\,\mathrm{d}\zeta\Bigg\}\Bigg], \tag{A.3b}$$

$$\frac{\sigma_{12}}{\tau_0}=\frac{1}{\pi R(v)}\left[4\alpha_1\alpha_s\sqrt{\frac{r_1}{L}}\cos\left(\frac{\theta_1}{2}\right)\left\{\int_0^1\frac{[\zeta+(r_1/L)]}{\sqrt{\zeta}[\zeta^2+(r_1/L)^2+2\zeta(r_1/L)\cos\theta_1]}\,\mathrm{d}\zeta\right.\right.$$
$$+\frac{\sin\gamma\pi}{\pi}\int_0^1\left(\frac{\zeta}{1-\zeta}\right)^{\gamma}\frac{[\zeta+(r_1/L)]}{[\zeta^2+(r_1/L)^2+2\zeta(r_1/L)\cos\theta_1]}$$
$$\left.\times\int_0^1\frac{(1-s)^{\gamma}}{\sqrt{s}(1-s\zeta)}\,\mathrm{d}s\,\mathrm{d}\zeta\right\}-(1+\alpha_s^2)^2\sqrt{\frac{r_s}{L}}\cos\left(\frac{\theta_s}{2}\right)$$
$$\times\left\{\int_0^1\frac{[\zeta-(r_s/L)]}{\sqrt{\zeta}[\zeta^2+(r_s/L)^2+2\zeta(r_s/L)\cos\theta_s]}\,\mathrm{d}\zeta+\frac{\sin\gamma\pi}{\pi}\int_0^1\left(\frac{\zeta}{1-\zeta}\right)^{\gamma}\right.$$
$$\left.\left.\times\frac{[\zeta+(r_s/L)]}{[\zeta^2+(r_s/L)^2+2\zeta(r_s/L)\cos\theta_s]}\int_0^1\frac{(1-s)^{\gamma}}{\sqrt{s}(1-s\zeta)}\,\mathrm{d}s\,\mathrm{d}\zeta\right\}\right]. \tag{A.3c}$$

For an intersonic mode II crack with a rate independent cohesive zone ($\beta=0$):

$$\frac{\sigma_{11}}{\tau_0}=\frac{\sin q\pi}{q\pi}\left[\frac{(1+2\alpha_1^2+\hat{\alpha}_s^2)}{2\alpha_1}\frac{1}{(r_1/L)^q}\right.$$
$$\times\left\{-\sin q\theta_1+q\int_0^1\frac{\zeta^q[\zeta\sin q\theta_1+(r_1/L)\sin(q+1)\theta_1]}{\zeta^2+(r_1/L)^2+2\zeta(r_1/L)\cos\theta_1}\,\mathrm{d}\zeta\right\}$$
$$-\frac{(1-\hat{\alpha}_s^2)}{2\alpha_1}\frac{\sin q\pi}{((-\eta_1-\hat{\alpha}_s\eta_2)/L)^q}$$
$$\left.\times\left\{-1+q\,\mathrm{pv}\int_0^1\frac{\zeta^q}{\zeta+((-\eta_1+\hat{\alpha}_s\eta_2)/L)}\,\mathrm{d}\zeta\right\}H(-\eta_1-\hat{\alpha}_s\eta_2)\right], \tag{A.4a}$$

$$\frac{\sigma_{22}}{\tau_0}=\frac{\sin q\pi}{q\pi}\left[\frac{-(1-\hat{\alpha}_s^2)}{2\alpha_1}\frac{1}{(r_1/L)^q}\right.$$
$$\times\left\{-\sin q\theta_1+q\int_0^1\frac{\zeta^q[\zeta\sin q\theta_1+(r_1/L)\sin(q+1)\theta_1]}{\zeta^2+(r_1/L)^2+2\zeta(r_1/L)\cos\theta_1}\,\mathrm{d}\zeta\right\}$$

$$+\frac{(1-\hat{\alpha}_s^2)}{2\alpha_1}\frac{\sin q\pi}{((-\eta_1-\hat{\alpha}_s\eta_2)/L)^q}$$

$$\times\left\{-1+q\,\mathrm{pv}\int_0^1\frac{\zeta^q}{\zeta+((-\eta_1+\hat{\alpha}_s\eta_2)/L)}\,\mathrm{d}\zeta\right\}H(-\eta_1-\hat{\alpha}_s\eta_2)\Bigg], \qquad (A.4b)$$

$$\frac{\sigma_{12}}{\tau_0}=\frac{\sin q\pi}{q\pi}\left[\frac{-1}{(r_1/L)^q}\left\{-\cos q\theta_1+q\int_0^1\frac{\zeta^q[\zeta\cos q\theta_1+(r_1/L)\cos(q+1)\theta_1]}{\zeta^2+(r_1/L)^2+2\zeta(r_1/L)\cos\theta_1}\,\mathrm{d}\zeta\right\}\right.$$

$$+\frac{\cos q\pi}{((-\eta_1-\hat{\alpha}_s\eta_2)/L)^q}\left\{-1+q\,\mathrm{pv}\int_0^1\frac{\zeta^q}{\zeta+((-\eta_1+\hat{\alpha}_s\eta_2)/L)}\,\mathrm{d}\zeta\right\}$$

$$\left.\times H(-\eta_1-\hat{\alpha}_s\eta_2)\right], \qquad (A.4c)$$

For an intersonic mode II crack with a rate-dependent cohesive zone ($\beta>0$):

$$\frac{\sigma_{11}}{\tau_0}=\frac{\sin q\pi}{2\pi\alpha_1}\left[(1+2\alpha_1^2+\hat{\alpha}_s^2)\left(\frac{r_1}{L}\right)^{1-q}\right.$$

$$\times\left\{\int_0^1\frac{[\zeta\sin(1-q)\theta_1-(r_1/L)\sin q\theta_1]}{\zeta^{1-q}[\zeta^2+(r_1/L)^2+2\zeta(r_1/L)\cos\theta_1]}\,\mathrm{d}\zeta+\frac{\sin\lambda\pi}{\pi}\int_0^1\left(\frac{\zeta}{1-\zeta}\right)^{\lambda}\right.$$

$$\left.\times\frac{[\zeta\sin(1-q)\theta_1-(r_1/L)\sin q\theta_1]}{[\zeta^2+(r_1/L)^2+2\zeta(r_1/L)\cos\theta_1]}\int_0^1\frac{(1-s)^{\lambda}}{s^q(1-s\zeta)}\,\mathrm{d}s\,\mathrm{d}\zeta\right\}$$

$$-(1-\hat{\alpha}_s^2)\sin q\pi\,\xi^{1-q}\left\{\int_0^1\frac{\mathrm{d}\zeta}{\zeta^{1-q}(\zeta-\xi)}+\int_0^1\frac{\mathrm{d}s}{s^q(1-s\xi)}\right.$$

$$\left.\left.-Q(\xi,\lambda)\int_0^1\frac{(1-s)^{\lambda}}{s^q(1-s\xi)}\,\mathrm{d}s\right\}H(\xi)\right], \qquad (A.5a)$$

$$\frac{\sigma_{22}}{\tau_0}=\frac{\sin q\pi}{2\pi\alpha_1}\left[-(1-\hat{\alpha}_s^2)\left(\frac{r_1}{L}\right)^{1-q}\right.$$

$$\times\left\{\int_0^1\frac{[\zeta\sin(1-q)\theta_1-(r_1/L)\sin q\theta_1]}{\zeta^{1-q}[\zeta^2+(r_1/L)^2+2\zeta(r_1/L)\cos\theta_1]}\,\mathrm{d}\zeta+\frac{\sin\lambda\pi}{\pi}\right.$$

$$\left.\left.\times\int_0^1\left(\frac{\zeta}{1-\zeta}\right)^{\lambda}\frac{[\zeta\sin(1-q)\theta_1-(r_1/L)\sin q\theta_1]}{[\zeta^2+(r_1/L)^2+2\zeta(r_1/L)\cos\theta_1]}\int_0^1\frac{(1-s)^{\lambda}}{s^q(1-s\zeta)}\,\mathrm{d}s\,\mathrm{d}\zeta\right\}\right.$$

$$+(1-\hat{\alpha}_s^2)\sin q\pi\xi^{1-q}\left\{\int_0^1 \frac{\mathrm{d}\zeta}{\zeta^{1-q}(\zeta-\xi)}+\int_0^1 \frac{\mathrm{d}s}{s^q(1-s\xi)}\right.$$

$$\left.-Q(\xi,\lambda)\int_0^1 \frac{(1-s)^\lambda}{s^q(1-s\xi)}\,\mathrm{d}s\right\}H(\xi)\Bigg], \tag{A.5b}$$

$$\frac{\sigma_{12}}{\tau_0}=\frac{\sin q\pi}{\pi}\left[\left(\frac{r_1}{L}\right)^{1-q}\left\{\int_0^1 \frac{[\zeta\cos(1-q)\theta_1+(r_1/L)\cos q\theta_1]}{\zeta^{1-q}[\zeta^2+(r_1/L)^2+2\zeta(r_1/L)\cos\theta_1]}\,\mathrm{d}\zeta\right.\right.$$

$$+\frac{\sin\lambda\pi}{\pi}\int_0^1\left(\frac{\zeta}{1-\zeta}\right)^\lambda\frac{[\zeta\cos(1-q)\theta_1+(r_1/L)\cos q\theta_1]}{[\zeta^2+(r_1/L)^2+2\zeta(r_1/L)\cos\theta_1]}$$

$$\left.\times\int_0^1\frac{(1-s)^\lambda}{s^q(1-s\zeta)}\,\mathrm{d}s\,\mathrm{d}\zeta\right\}+\cos q\pi\xi^{1-q}\left\{\int_0^1\frac{\mathrm{d}\zeta}{\zeta^{1-q}(\zeta-\xi)}+\int_0^1\frac{\mathrm{d}s}{s^q(1-s\xi)}\right.$$

$$\left.\left.-Q(\xi,\lambda)\int_0^1\frac{(1-s)^\lambda}{s^q(1-s\xi)}\,\mathrm{d}s\right\}H(\xi)\right], \tag{A.5c}$$

where

$$Q(\xi,\lambda)=\begin{cases}\cos\pi\lambda\left(\dfrac{\xi}{1-\xi}\right)^\lambda, & \xi<1,\\[2ex] \left(\dfrac{-\xi}{1-\xi}\right)^\lambda, & \xi>1,\end{cases} \tag{A.6a}$$

$$\xi=\frac{-\eta_1-\hat{\alpha}_s\eta_2}{L}. \tag{A.6b}$$

References

Abraham, F.F., Gao, H.J., 2000. How fast can cracks propagate? Phys. Rev. Lett. 84 (14), 3113–3116.

Andrews, D.J., 1976. Rupture velocity of plane strain shear cracks. J. Geophys. Res. 81 (32), 5679–5687.

Archuleta, R.J., 1984. A faulting model for the 1979 Imperial-valley earthquake. J. Geophys. Res. 89 (6), 4559–4585.

Bouchon, M., Toksöz, N., Karabulut, H., Bouin, M.P., Dietrich, M., Aktar, M., Edie, M., 2000. Seismic imaging of the 1999 Izmit (Turkey) rupture inferred from the near-fault recordings. Geophys. Res. Lett. 27 (18), 3013–3016.

Bouchon, M., Bouin, M.P., Karabulut, H., Toksöz, M.N., Dietrich, M., Rosakis, A.J., 2001. How fast is rupture during an earthquake? New insights from the 1999 Turkey earthquakes. Geophys. Res. Lett. 28 (14), 2723–2726.

Broberg, K.B., 1987. On crack paths. Eng. Fracture Mech. 28 (5–6), 663–679.

Broberg, K.B., 1989. The near-tip field at high crack velocities. Int. J. Fracture 39 (1–3), 1–13.

Broberg, K.B., 1994. Intersonic bilateral slip. Geophys. J. Int. 119 (3), 706–714.

Broberg, K.B., 1995. Intersonic mode II crack expansion. Arc. Mech. 47, 859–871.

Broberg, K.B., 1996. How fast can a crack go? Mater. Sci. 32 (1), 80–86.

Broberg, K.B., 1999a. Cracks and Fracture. Academic Press, London.
Broberg, K.B., 1999b. Intersonic mode II crack acceleration. Fatigue Fracture Eng. Mater. Struct. 22 (1), 17–24.
Burridge, R., 1973. Admissible speeds for plane strain shear cracks with friction but lacking cohesion. Geophys. J. Roy. Astron. Soc. 35, 439–455.
Burridge, R., Conn, G., Freund, L.B., 1979. The stability of a rapid mode II shear crack with finite cohesive traction. J. Geophys. Res. 85 (B5), 2210–2222.
Coker, D., Rosakis, A.J., 2001. Experimental observations of intersonic crack growth in asymmetrically loaded unidirectional composite plates. Philos. Mag. 81 (3), 571–595.
Cotterell, B., Rice, J.R., 1980. Slightly curved or kinked cracks. Int. J. Fracture 16, 155–169.
Curran, D.A., Shockey, D.A., Winkler, S., 1970. Crack propagation at supersonic velocities—II. Theoretical model. Int. J. Fracture Mech. 6 (3), 271–278.
Dally, J.W., Riley, W.F., 1991. Experimental Stress Analysis. McGraw-Hill, New York.
Das, S., 1985. Application of dynamic shear crack models to the study of the earthquake faulting process. Int. J. Fracture 27 (3–4), 263–276.
Das, S., Aki, K., 1977. A numerical study of two-dimensional spontaneous rupture propagation. Geophys. J. Roy. Astron. Soc. 50, 643–668.
Dmowska, R., Rice, J.R., 1986. Fracture theory and its seismological applications. In: Teisseyre, R. (Ed.), Continuum Theories in Solid Earth Physics. Elsevier, Amsterdam, pp. 187–255.
Ellsworth, W.L., Celebi, M., 1999. Near-field displacement time histories of the M 7.4 Kocaeli (Izimit), Turkey, earthquake of August 17, 1999. In: AGU99 Fall Meeting, San Fransisco, CA.
Fineberg, J., Marder, M., 1999. Instability in dynamic fracture. Phys. Rep. 313 (1–2), 2–108.
Freund, L.B., 1979. The mechanics of dynamic shear crack propagation. J. Geophys. Res. 84 (B5), 2199–2209.
Freund, L.B., 1990. Dynamic Fracture Mechanics. Cambridge University Press, Cambridge.
Freund, L.B., Lee, Y.J., 1990. Observations on high strain rate crack growth based on a strip yield model. Int. J. Fracture 42 (3), 261–276.
Gakhov, F.D., 1990. Boundary Value Problems. Dover, New York.
Gao, H., Huang, Y., Gumbsch, P., Rosakis, A.J., 1999. On radiation-free transonic motion of cracks and dislocations. J. Mech. Phys. Solids 47 (9), 1941–1961.
Gao, H., Huang, Y., Abraham, F.A., 2001. Continuum and atomistic studies of intersonic crack propagation. J. Mech. Phys. Solids 49 (9), 2113–2132.
Gao, H.J., 1993. Surface roughening and branching instabilities in dynamic fracture. J. Mech. Phys. Solids 41, 457–486.
Georgiadis, H.G., 1986. On the stress singularity in steady-state transonic shear crack propagation. Int. J. Fracture 30 (3), 175–180.
Geubelle, P.H., Kubair, D., 2001. Intersonic crack propagation in homogeneous media under shear dominated loading—numerical analysis. J. Mech. Phys. Solids 49 (3), 571–587.
Glennie, E.B., 1971a. A strain-rate dependent crack model. J. Mech. Phys. Solids 19, 255–272.
Glennie, E.B., 1971b. The unsteady motion of a rate-dependent crack model. J. Mech. Phys. Solids 19, 329–338.
Hernandez, B., Cotton, F., Campillo, M., 1999. Contribution of radar interferometry to a two-step inversion of the kinematic process of the 1992 Landers earthquake. J. Geophys. Res. 104 (B6), 13 083–13 099.
Huang, Y., Gao, H., 2001. Intersonic crack propagation—part I: the fundamental solution. J. Appl. Mech. 68 (2), 169–175.
Huang, Y., Wang, W., Liu, C., Rosakis, A.J., 1999. Analysis of intersonic crack growth in unidirectional fiber-reinforced composites. J. Mech. Phys. Solids 47 (9), 1893–1916.
Hutchinson, J.W., Suo, Z., 1992. Mixed-mode cracking in layered materials. Adv. Appl. Mech. 29, 63–191.
Ida, Y., 1972. Cohesive force across the tip of a longitudinal-shear crack and Griffith's specific surface energy. J. Geophys. Res. 77 (20), 3796–3805.
Johnson, E., 1990. On the initiation of unidirectional slip. Geophys. J. Int. 101 (1), 125–132.
Johnson, E., 1992. Process region changes for rapidly propagating cracks. Int. J. Fracture 55 (1), 47–63.
Lambros, J., Rosakis, A.J., 1995. Shear dominated transonic interfacial crack growth in a bimaterial. 1. Experimental observations. J. Mech. Phys. Solids 43 (2), 169–188.

Lee, Y.J., Freund, L.B., 1990. Fracture initiation due to asymmetric impact loading of an edge cracked plate. J. Appl. Mech. 57 (1), 104–111.

Lee, O.S., Knauss, W.G., 1989. Dynamic crack propagation along a weakly bonded plane in a polymer. Exp. Mech. 29 (3), 342–345.

Liu, C., Huang, Y., Rosakis, A.J., 1995. Shear dominated transonic interfacial crack growth in a bimaterial. 2. Asymptotic fields and favorable velocity regimes. J. Mech. Phys. Solids 43 (2), 189–206.

Mason, J.J., Lambros, J., Rosakis, A.J., 1992. The use of a coherent gradient sensor in dynamic mixed mode fracture mechanics experiments. J. Mech. Phys. Solids 40 (3), 641–661.

Melin, S., 1986. When does a crack grow under mode II conditions. Int. J. Fracture 30 (2), 103–114.

Muskhelishvili, N.I., 1963. Some Basic Problems of the Mathematical Theory of Elasticity, 4th Edition. Noordhoff, Groningen, Holland.

Needleman, A., 1999. An analysis of intersonic crack growth under shear loading. J. Appl. Mech. 66 (4), 847–857.

Nematnasser, S., Horii, H., 1982. Compression-induced nonplanar crack extension with application to splitting, exfoliation, and rockburst. J. Geophys. Res. 87 (B8), 6805–6821.

Olsen, K.B., Madariaga, R., Archuleta, R.J., 1997. Three-dimensional dynamic simulation of the 1992 Landers earthquake. Science 278 (5339), 834–838.

Palmer, A.C., Rice, J.R., 1973. The growth of slip surfaces in the progressive failure of over-consolidated clay. Proc. Roy. Soc. London A 332, 527–548.

Ramulu, M., Kobayashi, A.S., 1985. Mechanics of crack curving and branching — a dynamic fracture analysis. Int. J. Fracture 27 (3–4), 187–201.

Ravichandar, K., Knauss, W.G., 1984a. An experimental investigation into dynamic fracture. 3. On steady-state crack propagation and crack branching. Int. J. Fracture 26 (2), 141–154.

Ravichandar, K., Knauss, W.G., 1984b. An experimental investigation into dynamic fracture. 2. Microstructural aspects. Int. J. Fracture 26 (1), 65–80.

Rice, J.R., 1980. The mechanics of earthquake rupture. In: Boschi, E. (Ed.), Physics of the Earth's Interior. North-Holland, Amsterdam, pp. 555–649.

Rosakis, A.J., Samudrala, O., Coker, D., 1999. Cracks faster than the shear wave speed. Science 284 (5418), 1337–1340.

Rosakis, A.J., Samudrala, O., Singh, R.P., Shukla, A., 1998. Intersonic crack propagation in bimaterial systems. J. Mech. Phys. Solids 46 (10), 1789–1813.

Rosakis, A.J., Samudrala, O., Coker, D., 2000. Intersonic shear crack growth along weak planes. Mater. Res. Innovations 3 (4), 236–243.

Schardin, H., 1959. Velocity effects in fracture. In: Averback, B.L. (Ed.), Fracture. Wiley, New York, pp. 121–1232.

Singh, R.P., Lambros, J., Shukla, A., Rosakis, A.J., 1997. Investigation of the mechanics of intersonic crack propagation along a bimaterial interface using coherent gradient sensing and photoelasticity. Proc. Roy. Soc. London A 453 (1967), 2649–2667.

Spudich, P., Cranswick, E., 1984. Direct observation of rupture propagation during the 1979 Imperial valley earthquake using a short baseline accelerometer array. Bull. Seismol. Soc. Amer. 74, 2083–2114.

Washabaugh, P.D., Knauss, W.G., 1994. A reconciliation of dynamic crack velocity and Rayleigh wave speed in isotropic brittle solids. Int. J. Fracture 65 (2), 97–114.

Winkler, S., Shockey, D.A., Curran, D.A., 1970. Crack propagation at supersonic velocities—I. Int. J. Fracture Mech. 6 (2), 151–158.

Yu, H.H., Suo, Z., 2000. Intersonic crack growth on an interface. Proc. Roy. Soc. London A 456 (1993), 223–246.